Antonio Ciriello, Bsc

The internal structure of the Millstatt Complex and its tectonometamorphic evolution (Carinthia, Eastern Alps)

MASTERARBEIT

zur Erlangung des akademischen Grades

Master of Science

Masterstudium Erdwissenschaften

eingereicht an der

Technischen Universität Graz

Betreuer

Priv.-Doz. Mag. Dr.rer.nat. Krenn Kurt

Institut für Erdwissenschaften

Graz, März 2017

EIDESSTATTLICHE ERKLÄRUNG

AFFIDAVIT

Ich erkläre an Eides statt, dass ich die vorliegende Arbeit selbstständig verfasst, andere als die angegebenen Quellen/Hilfsmittel nicht benutzt, und die den benutzten Quellen wörtlich und inhaltlich entnommenen Stellen als solche kenntlich gemacht habe. Das in TUGRAZonline hochgeladene Textdokument ist mit der vorliegenden Masterarbeit identisch.

I declare that I have authored this thesis independently, that I have not used other than the declared sources/resources, and that I have explicitly indicated all material which has been quoted either literally or by content from the sources used. The text document uploaded to TUGRAZonline is identical to the present master's thesis.

Datum / Date	Unterschrift / Signature

Acknowledgements

In the first place I want to thank my supervisor Prof. Kurt Krenn for his great support and long discussions that helped me to accomplish this thesis. Furthermore I want to thank Prof. Georg Hoinkes for his encouraging words and comments on the thesis.

I thank Prof. Karl Ettinger for helping me with the SEM, Anton Pock for polishing the thin sections, as well as all the staff members.

Special thanks also to my colleagues, Sara Raič and Dragan Jutric for their help in the field and fruitful comments to the thesis.

Many many thanks also to all my classmates and buddies who made this part of my life memorable, at university and beyond. Thank you: Paul, Luki, Felix, Plesche, Sarah, Mani, Tine, Leo, Stefan, Stevo, Flo, Erich, Lisa, Berni, Tomml, Honnä, Luggi, Eugen, Sevi, Gaby, Eli and Pablo.

Last but not least I thank my parents for their unconditional love and support throughout my studies. It means the world to me. **Thank you.**

Abstract

The Millstatt Complex (MC, Carinthia, Austria) is part of the Koralpe-Wölz high-pressure nappe system, east of the Tauern Window. It contains former eclogites in the vicinity of tremolite-bearing marbles at the footwall and staurolite-bearing garnet – micaschists towards the hangingwall. Using field structural mapping together with petrographic and microstructural analysis, the major aim of this study is to characterize the internal architecture of the MC. In general, the MC represents a SSW-vergent large-scale fold structure which experienced eo-Alpine deformation and subsequent Alpine overprint. Early tight fold structures embedded in a penetrative field foliation are mainly preserved in amphibolites of central areas of the MC. Garnet micaschists are dominantly arranged as m-shape fold structures characterizing large-scale fold hinge areas. Microstructures related to early stages exhibit syn-kinematically grown garnets as well as coaxial pressure shadows. Both structures are related to exhumation of the eo-Alpine wedge after peak metamorphism at ~100Ma. The final fold structure was later re-oriented due to Alpine indentation tectonics which leads to the present day internal structure. In addition, garnet major element zonation patterns have been obtained to distinguish between distinct metamorphic events and result into the definition of a typical “Laas type” zonation garnet which is already documented in comparable areas west of the Tauern Window. On the basis of further studies, and the new elaborated data it is proposed that the MC is part of the Laas unit west of the Tauern Window, separated from a nappe unit in the footwall, the Texel Complex.

Zusammenfassung

Der Millstatt Komplex (MC) ist Teil des Koralpe-Wölz Hochdruckdeckensystems, östlich des Tauernfensters. Dieser Komplex besteht unter anderem aus retrograden Eklogiten, benachbart von Tremolit-Marmoren im Liegenden und Staurolit-Granat Glimmerschiefern im Hangenden. Ziel dieser Arbeit ist es mittels Feldkartierung und petrographischer als auch mikrostruktureller Untersuchungen den internen Aufbau des MC zu charakterisieren. Generell stellt der MC eine großräumige SSW-vergente Faltenstruktur dar, die durch die eo-Alpine Orogenese und nachfolgender Alpiner Überprägung gebildet worden ist. Frühe, enge Faltenstrukturen wurden von einer penetrativen Schieferung überprägt, welche großteils in Amphiboliten im zentralen Bereich des MC aufgeschlossen sind. Granat-Glimmerschiefer sind, nahe den Faltenscheiteln, meist in einer „M“-Struktur angeordnet. Mikrostrukturen zeigen syn-kinematisch gewachsene Granate mit symmetrischen Druckschatten. Beide Strukturen stehen im Zusammenhang mit der Exhumierung des eo-Alpinen Hochdruckgürtels, nach dem Höhepunkt der Metamorphose um ~100 Ma. Die eo-Alpine Faltenstruktur wurde später durch die Alpine Indentertektonik umorientiert. Um metamorphe Ereignisse zu unterscheiden wurden zusätzlich Granatprofile erstellt. Diese ergaben ein charakteristisches „Laas-Typ“ Granatprofil, welches bereits in vergleichbaren Gebieten westlich des Tauernfensters beschrieben worden ist. Auf der Basis von weiteren Studien, und der Ergebnisse dieser Studie wird vorgeschlagen, dass der MC Teil der Laaser Serie im Westen des Tauernfensters ist und beide vom Texel Komplex im Liegenden als eigene eo-Alpine Decke abgegrenzt werden können.

Introduction

The Millstatt Complex (MC) is a polymetamorphic unit located in the Eastern Alps. It is attributed to the Eo-alpine Koralpe-Wölz high-pressure nappe system which is structurally located between the Silvretta-Seckau Nappe System in the footwall and the Ötztal-Bundschuh Nappe System in the hangingwall (Schuster et al., 2004; Schmid et al., 2004).

Previous studies by Schimana (1986) and Strauss (1990) describe basically the polymetamorphic character of the Millstatt area. On the basis of detailed petrography and geothermobarometry, Teiml (1996) described an increasing metamorphic field gradient towards the southern parts of the MC. Eclogites reached minimum P/T conditions from 600 - 630°C at 12-14 kbar, thus also defining the Southern Limit of Alpine Metamorphism in this area of the Eastern Alps (SAM; Hoinkes et al., 1999) extending from the Drautal to the southeastern end of the MC.

However, there exist only very few studies about the structural architecture of the MC, which holds the major aim of this study. In order to establish a tectonic evolution of the MC, structures were studied along selected profiles. For additional microstructural analysis representative samples have been taken for shear senses, rheology as well as the paragenetic evolution of coexisting mineral assemblages. The metamorphic character of the complex is explained on the basis of major element profiles of representative zoned garnet crystals. Preparation of samples and mineral chemical analysis were carried out at the University of Graz, Institute of Earth Sciences, Department of Petrology and Geochemistry.

1. Geological Overview

1.1 Introduction to the Alpine orogen

The complex Alpine orogen evolved from the still ongoing convergence between the European and the African plates and their incorporated microplates (continental and oceanic) (Handy et al., 2010) (Fig. 1). For the present-day structure of the Alpine arc, four main tectonic events since the eo-Alpine evolution are of major importance and mentioned here: (1) An intracontinental subduction zone within the Apulian plate generated the "Eo-Alpine High Pressure Belt" in the Early Cretaceous. (2) Subsequent extensional tectonics in the Late Cretaceous at ca. 80 Ma developed E to SE dipping faults accompanied with the formation of extensional basins (e.g. Gosau basins like Krappfeld Gosau or Gosau of Kainach) at the vicinity of nappe contacts. (3) A second compressive event in Tertiary times, characterized by WNW indentation of the "Apulian microplate" towards the Eastern Alps. (4) Since Early Oligocene, the compressive realm led to E-directed block extrusion between the Periadriatic Lineament (PAL) in the south and the Selztal - Ennstal – Mariazell – Puchegg Line (SEMP) in the north accompanied with vertical shortening in the Eastern Alps (Froitzheim et al., 1994; Schmid et al., 2004; Handy et al., 2010).

1.2 Eastern Alps

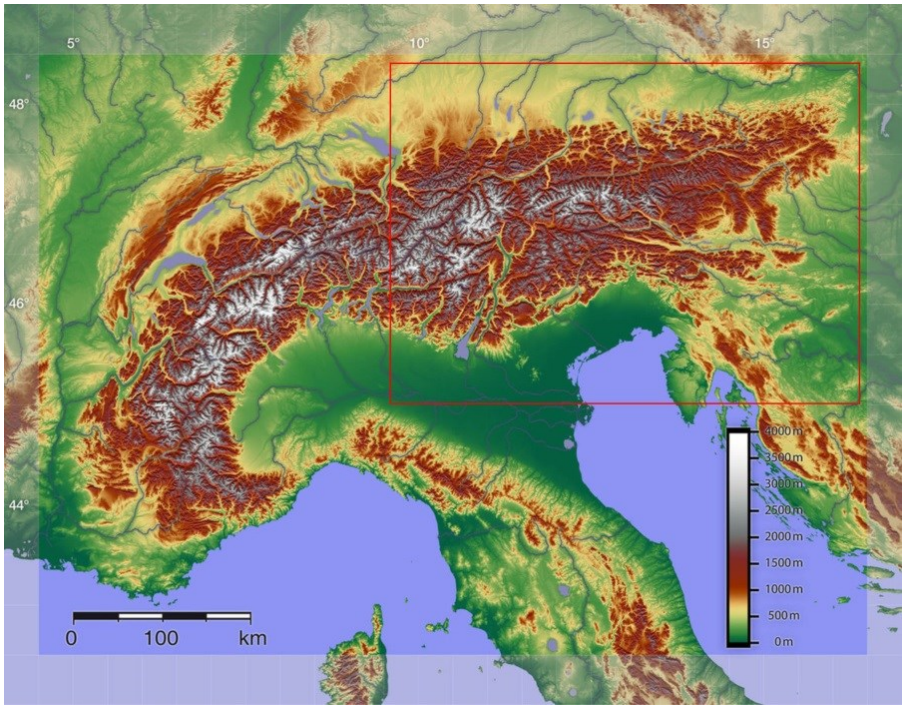

Fig 1| Topographic map of the Alpine orogen; Red square approximates the area of the Eastern Alps.

The Eastern Alps represent a complex architecture of Penninic-, Subpenninic-, Austroalpine- and Alpine foreland units. The structurally highest units are the Austroalpine nappes which are divided into Upper and Lower Austroalpine units, each consisting of basement and cover sequences (Schmid et al., 2004).

The Upper Austroalpine cover comprises Mesozoic sediments of the Northern Calcareous Alps (NCA) and the Grauwacke zone (GWZ). These units have been decoupled from their initial setting, the eastern Meliata Ocean, and thrusted to the north during subduction of the Meliata Ocean in Late Jurassic times. The NCA consist of two major nappes, the Juvavic and the Tyrolic, which are found today in an out-of-sequence fold and thrust belt at the northern margin of the Austroalpine units (Janàk et al., 2004). The Bavarian nappes represent more proximal Mesozoic cover sequences. The GWZ represents the former basement of the Tyrolic nappe system, once located north of the Meliata Ocean.

After Schmid et al. (2004) the Upper Austroalpine basement units include, from the structurally highest to the lowest, the Drauzug-Gurktal nappe system (DGN), the Ötztal-Bundschuh nappe system (ÖBN), the Koralpe-Wölz nappe system (KWNS) and the Silvretta-Seckau nappe system (SSN; Figs. 2 and 5).

Within the Eastern Alps, the DGN system includes various units: the Tonale series, the Meran-Mauls basement, the Gailtal basement, the Deferegger Alps, the Strieden basement, the Gurktal nappe, the Graz Paleozoic and the Steinach nappe. The eo-Alpine metamorphic imprint is rather low within these units, and can be compared with units south of the SAM-line, the southern Alpine units and the Dinarides. These nappes are considered as derived from the southern border of the Meliata embayment.

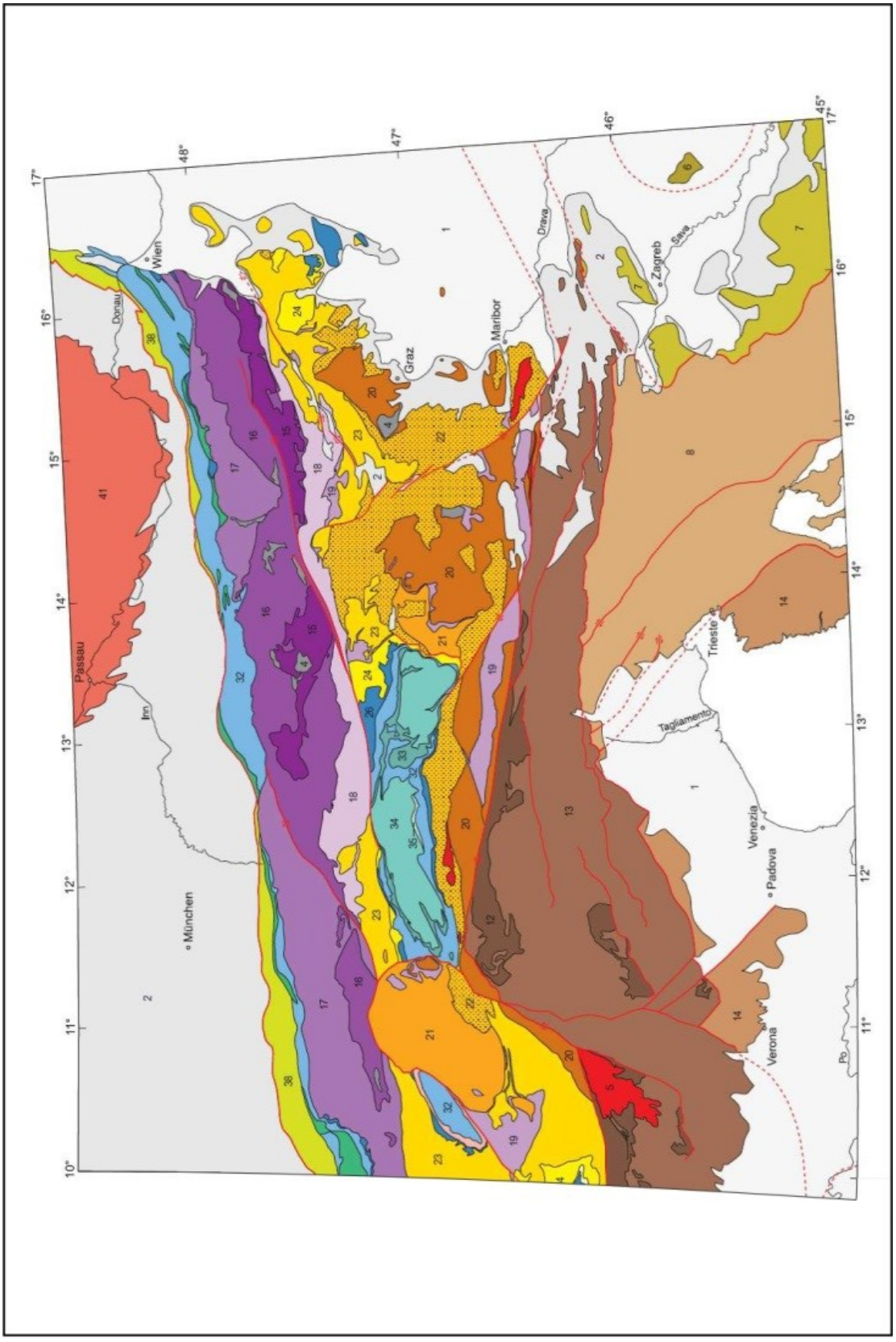
Wien
Donau
Graz
Maribor
Drava
Zagreb
Sava
Passau
Inn
München
Trieste
Tagliamento
Venezia
Padova
Verona
Po

Fig 2| Tectonic map of the Eastern Alps, after Schmid et al. (2004)

The ÖBN system is represented by the Ötztal-Stubaital nappe west, and the Bundschuh nappe east of the Tauern Window (TW). These nappes were connected as one crystalline unit prior to the unroofing and exhumation of the TW in Late Oligocene (Kurz et al., 2008). Both nappes show a polymetamorphic character, similar lithologies and ages, as well as an increasing metamorphic field gradient towards their footwall units (Schmid et al., 2004).

The lowest unit within the Upper Austroalpine nappe stack is the Silvretta Seckau nappe system, belonging to the basement unit at the northern margin of the Meliata embayment. The nappes attributed to this system are the Seckau crystalline nappe, the Schladming nappe, the Innsbrucker Quartzphyllite zone and the Semmering nappe in the east.

Lower Austroalpine basement units are only locally found in the Radstätter Tauern, surrounding the Tauern Window, and in the Wechsel Group in the East. They represent distal domains, once located on the passive margin between the Apulian Plate and the Piemont-Ligurian Ocean (Schmid et al., 2004).

The Penninic Units comprise slices of the Valais Ocean, the Briançonnais terrane and the Piemont-Ligurian Ocean and are subdivided into the Upper, Middle and Lower Penninic nappes. The Upper Penninic nappes derived from the Piemont-Ligurian Ocean and the accretionary wedge at the southern margin of the Alpine Tethys. The Middle Penninic nappes are only present in the Western and Central Alps, and are attributed to the Briançonnais microcontinent. The Lower Penninic nappes comprise the Rhenodanubian flysch zone, at the northern margin of the Autroalpine units in the Eastern Alps and calcic flyschoid sediments as well as meta-ophiolites in the Glockner nappe system of the Tauern Window and the Rechnitz Window (Schmid et al., 2004).

Units derived from the Variscan metamorphic continental crust are attributed to the Sub-Penninicum, a basement series that is found at the northern margin of the Austroalpine domain and in the lowermost units of the Tauern Window, summarized as Venediger Nappe Complex. (Kurz et al., 2001).

1.3 Paleogeographic Evolution

During the Early Jurassic, the Atlantic ocean starts to affect the Alpine realm in the east by the opening of the Piemont - Ligurian Ocean Basin (future Alpine Tethys after Schmid et al. 2004; Fig. 3a). This intracontinental spreading zone lasts from the Mid Jurassic to the Mid Eocene, where it was subducted to the S under the Apulian microplate.

With this spreading process a sinistral proto-periadriatic transform system developed within the Alpine Tethys, separating the Adriatic plate from the Alcapia and Tisza plates in the East, and creating a sinistral offset between the Western Ligurian and the Eastern Piedmont Oceans (Fig. 3a).

In the Early Cretaceous the spreading of the Northern Atlantic Ocean proceeded resulting into a sinistral transform system in the NE of the Iberian Peninsula by opening the Bay of Biscay (Fig. 3b). At 84 Ma, the Iberian plate is separated from the European plate and the transform system connects to the Periadriatic Transform System, as well as to the newly opened Valais Ocean to the NE of the Piedmont Ocean, holding the continental Briançonnais fragment in between. As a result, the Iberian plate moved eastwards along with subduction of the East-Ligurian Ocean towards the SE.

Simultaneously at the northern part of the Adriatic plate, an intracontinental subduction began by the early stages of eo-Alpine orogeny from 100 Ma onwards resulting in peak metamorphic ages between 95 – 85Ma (Fig. 3b). After Handy et al. (2010), the subduction zone is argued to be triggered by the pull of the Neotethyan slab, underlying the northern part of the Adriatic plate.

With the ongoing propagation of the subducting slab towards the NW, the Piedmont Ocean and the Briançonnais continental fragment are being incorporated in the accretionary wedge during the Cretaceous orogenic period, as well as the Valais Ocean and distal parts of the European margin at a later stage in Late Paleogene time (Figs. 3c, d; Froitzheim, 1994).

These two distinct collisional events were both followed by extensional tectonics. An early event in Late Cretaceous (~ 80Ma) and a later event in Late Eocene (~35 Ma). The first extensional event led to the development of the Gosau Group, a sedimentary sequence found in E and SE directed normal-fault basins, attributed to overall thinning of the orogenic lithosphere (Handy et al., 2010). The second extensional event occurred just after the break-off of the subducted Adriatic plate, between 35 and 25Ma (Late Eocene – Early Oligocene)

which resulted in exhumation of the Penninic units and lateral E – directed extrusion within the Eastern Alps.

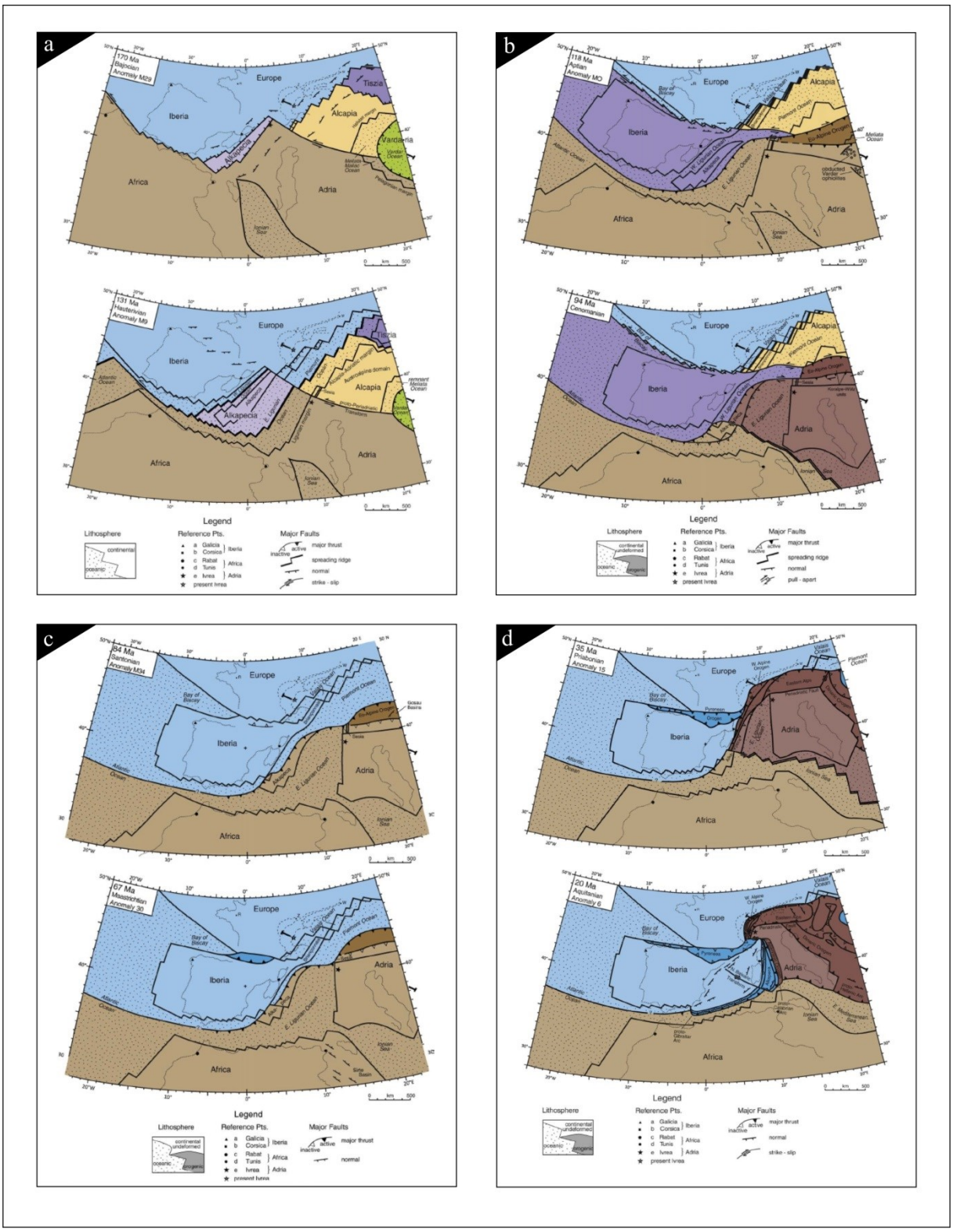

Fig. 3| a) – d) Paleogeographic reconstruction of the Alps from Mid Jurassic to Early Neogene after Handy et al. (2010).

2. Regional Geology

2.1 The Koralpe-Wölz high-pressure nappe system

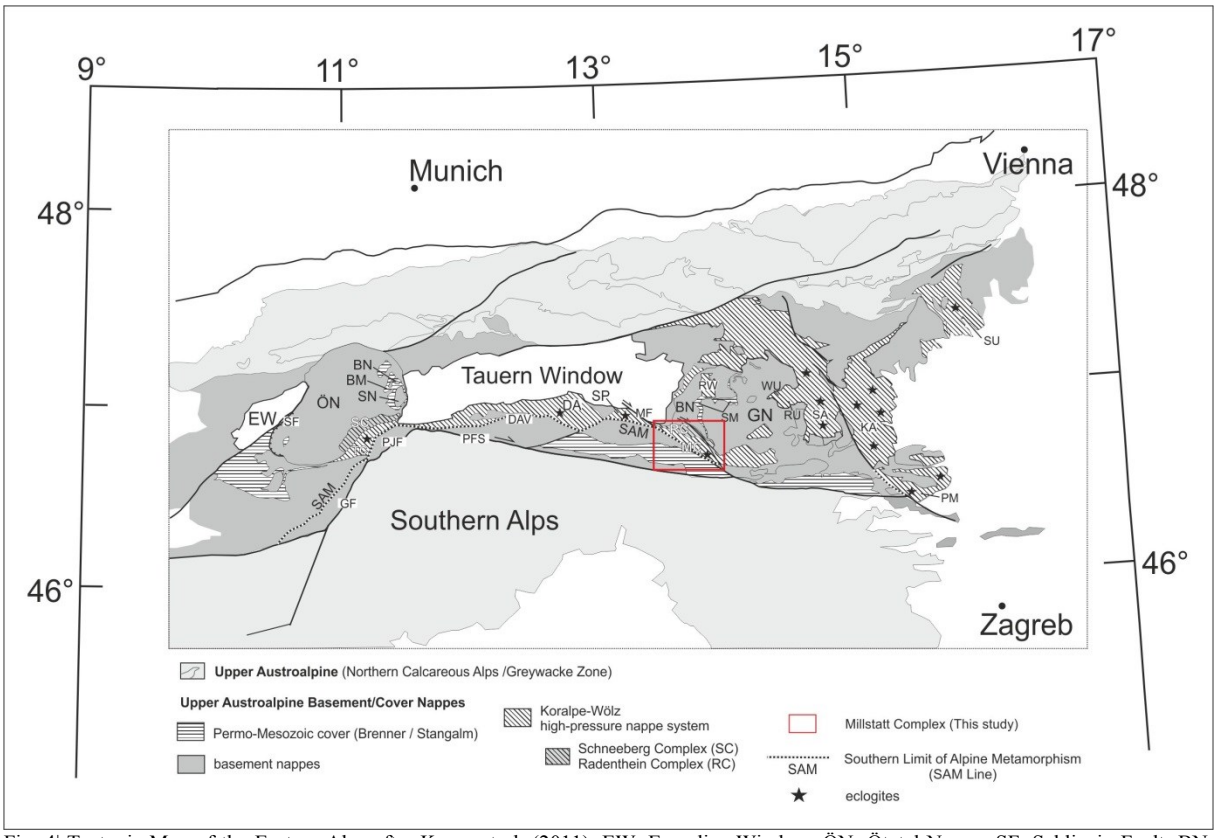

Fig. 4| Tectonic Map of the Eastern Alps after Krenn et al. (2011). EW: Engadine Window; ÖN: Ötztal Nappe; SF: Schlienig Fault; BN: Bundschuh Nappe ; BM: Brenner Mesozoic; SN: Steinach Nappe; GF: Giudicarie Fault; PJF: Passaier-Jaufen Fault; PFS: Periadriatic Fault System; DAV: Defreggen-Antholz-Vals Fault; DA: Deferegger Alps; SP: Schober-Polinik Unit; MF: Mölltal Fault; SM: Stangalm Mesozoic; GN: Gurktal Nappe; RW: Ramingstein Window; SA: Saualpe Nappe; WU: Wölz Unit; RU: Rappold Unit; KA: Koralm Nappe; PM: Pohorje Mountains; SU: Strallegg Unit

The Early Cretaceous subduction resulted into the eo-Alpine metamorphic imprint in the Austroalpine units. It is represented by pressure dominated (eclogite facies, Fig. 5) metamorphism and subsequent decompressive regional metamorphism (amphibolite facies).

Evidence for ultra-high pressure (UHP) metamorphism is documented in the Pohorje Mountains in Slovenia. There, kyanite-bearing eclogites, represent the deepest units of the subducted material (Janàk et al., 2004). East of the Tauern Window, the KWNS extends from the Pohorje Mountains to the Koralm-Saualm unit towards NW including the Wölz and Rappold Units (Fig. 4). Northeast of the Koralm-Saualm unit, the Strallegg Unit, with its adjacent units, are also attributed to the KWNS.

Southeast of the Tauern Window the Millstatt Complex (MC) is located, holding the monometamorphic Radenthein Complex (RC) in the hangingwall position. To the south of the TW the Schober-Polinik Unit and the northern Deferegger Alps are also attributed to the

KWNS. West of the TW, the westernmost units comprise the Texel Complex with the monometamorphic Schneeberg Complex in the hangingwall.

In contrast to the overlying Bundschuh Complex, the nappes of the KWNS were not all affected by Variscan metamorphism. The units of the KWNS show a polymetamorphic character, generated by Permian and eo-Alpine metamorphic events.

Most of the units within the KWNS contain eo-Alpine eclogites, constraining P/T conditions and subduction depth estimates. Latest data from the Texel Complex yield minimum P/T conditions of 600°C and 13 GPa (Habler et al., 2006), which correspond to ~40 km of burial depth for this portion of the subduction zone. The eclogites in the Pohorje Mountains were buried to depths of about 90-100km (Janák et al., 2004) and experienced P/T-conditions of ca. 800°C and ~ 3 GPa.

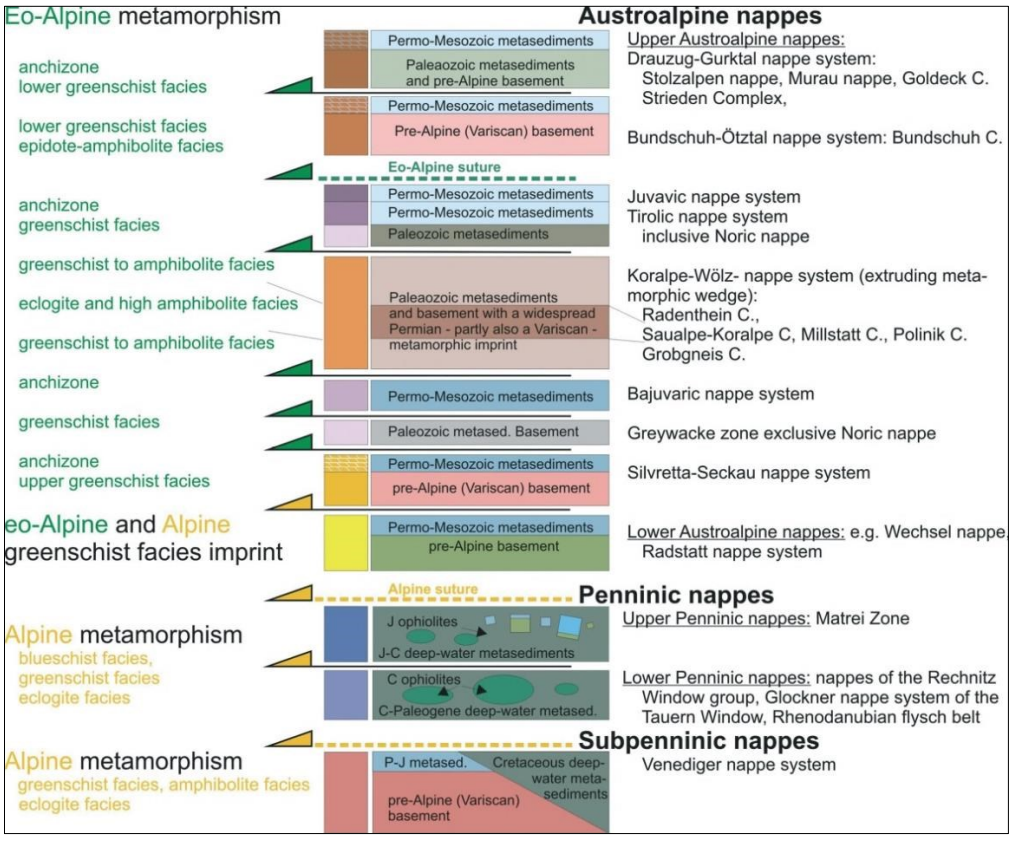

Fig. 5| Tectonostratigraphy of the Eastern Alps, including eo-Alpine and Alpine metamorphic events (after Schuster et al., 2004).

2.2 The Millstatt Complex

The investigated area lies within the KWNS (Fig. 5). To the south, the Millstatt Complex is bordered by the dextral Mölltal fault (MF), which is linked to the Periadriatic Fault System (PFS Fig. 4) further to the southeast. At the hangingwall of the MC, the monometamorphic Radenthein Complex (RC) is exposed. The polymetamorphic Bundschuh Complex (BN), as part of the ÖBN system, overlies the RC to the north and northeast. The MC and the BC underwent a polymetamorphic evolution, whereas the RC contrasts by eo-Alpine mono-metamorphism (Hoinkes et al., 1999). It may represent a former sedimentary cover sequence of Paleozoic age in the hangingwall position of the MC (Schuster et al., 2003).

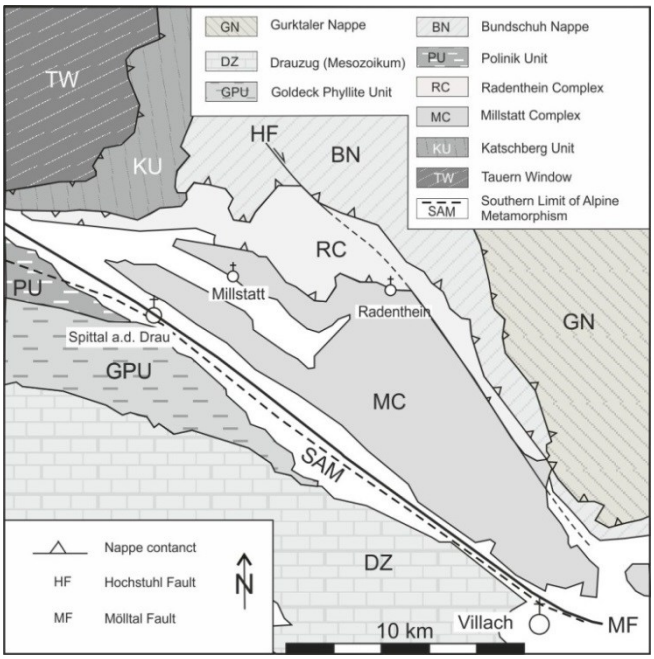

Fig. 6| Tectonic map of the Austroalpine Units east of the Tauern Window after Krenn et al., 2011.

The lithostratigraphy of the MC consists of garnet - micaschists, marbles and garnet - amphibolite lenses at the footwall, followed by st-garnet - micaschists and smaller amphibolite lenses. To the hangingwall the MC consists of phyllonitic garnet - micaschists and quartzitic units, also with amphibolites and marble intercalations. Concordant pegmatite intrusions, of Permian age, are found throughout the stratigraphic sequence (Schuster & Frank, 1999). The amphibolite bodies show eclogitic garnet-amphibolite assemblages where relictic omphacite has been described at lower levels (Teiml et al., 1996). Retrogressed garnet amphibolites include symplectitic textures consisting of plagioclase and amphibole. Adjacent to the marbles, metamorphic calcsilicate rocks occur. Lenses of marbles occur in almost all lithologies, with the largest being the "Puch-Weißensteiner Marmorzug" near the village Gummern, where various quarries have been constructed. These rocks are coarse-grained and show tremolite-bearing mineral assemblages.

3. Study area in detail

The investigated area is located in Upper Carinthia, northwest to the city Villach in the north of the Drau valley, where it extends near to Spittal a.d. Drau in the west and to Radenthein in the north. The highest point is the Mirnock summit (2110m). The total area covers about 300 km^2.

The study area is covered with quaternary sediments derived from the last glacial event. Lower levels present lesser representative outcrops, whereas at higher levels, outcrops occur more frequently, making profiling possible. Samples from observed lithologies have been collected and their corresponding thin sections were cut parallel to the stretching lineation to investigate microstructures and related shear sense directions.

3.1 Sample locations

The map in Fig. 7 shows the GPS locations of the sampled rock material, as well as four study areas A to D.

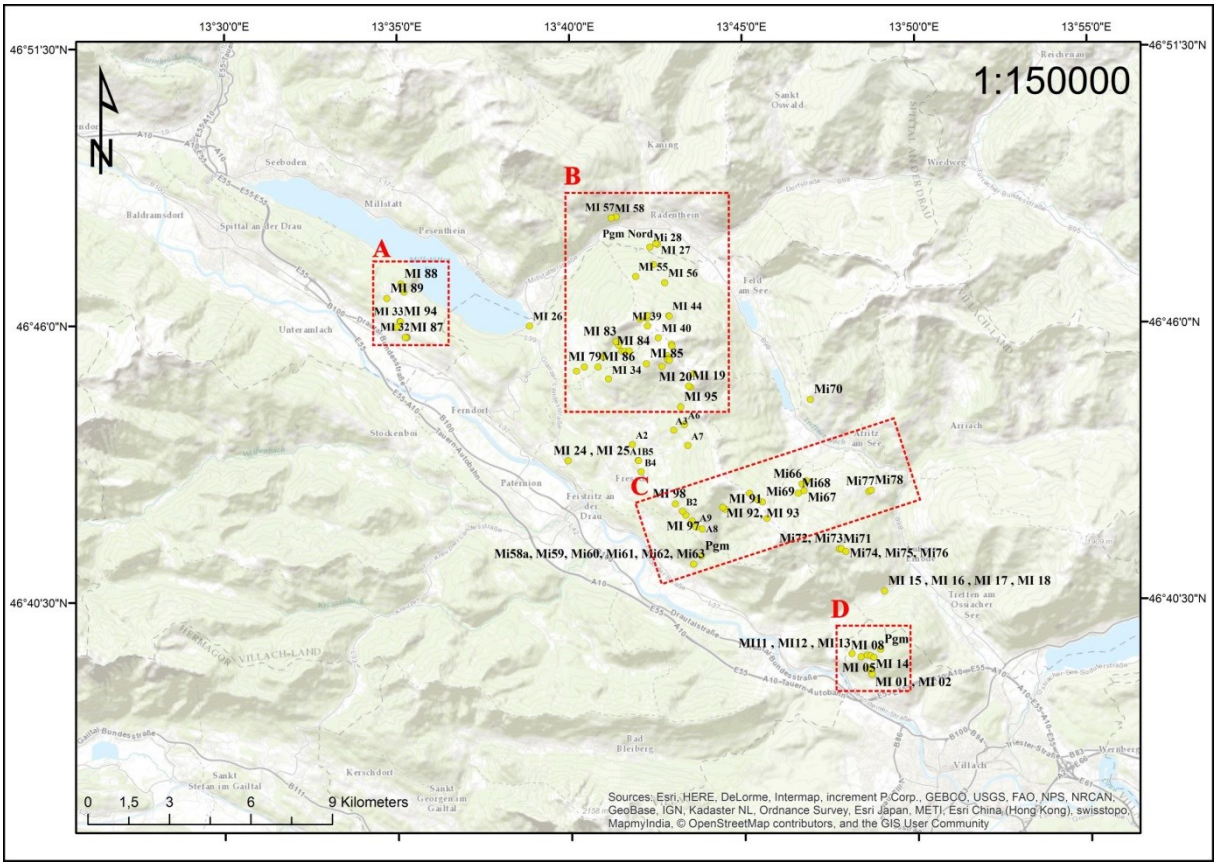

Fig. 7| Topographic map of the study area including sample locations; Red rectangles indicate four study areas A to D.

3.2 Structural field data

Figures 8 - 11 include mapped lithologies and structural field data from study areas A to D.

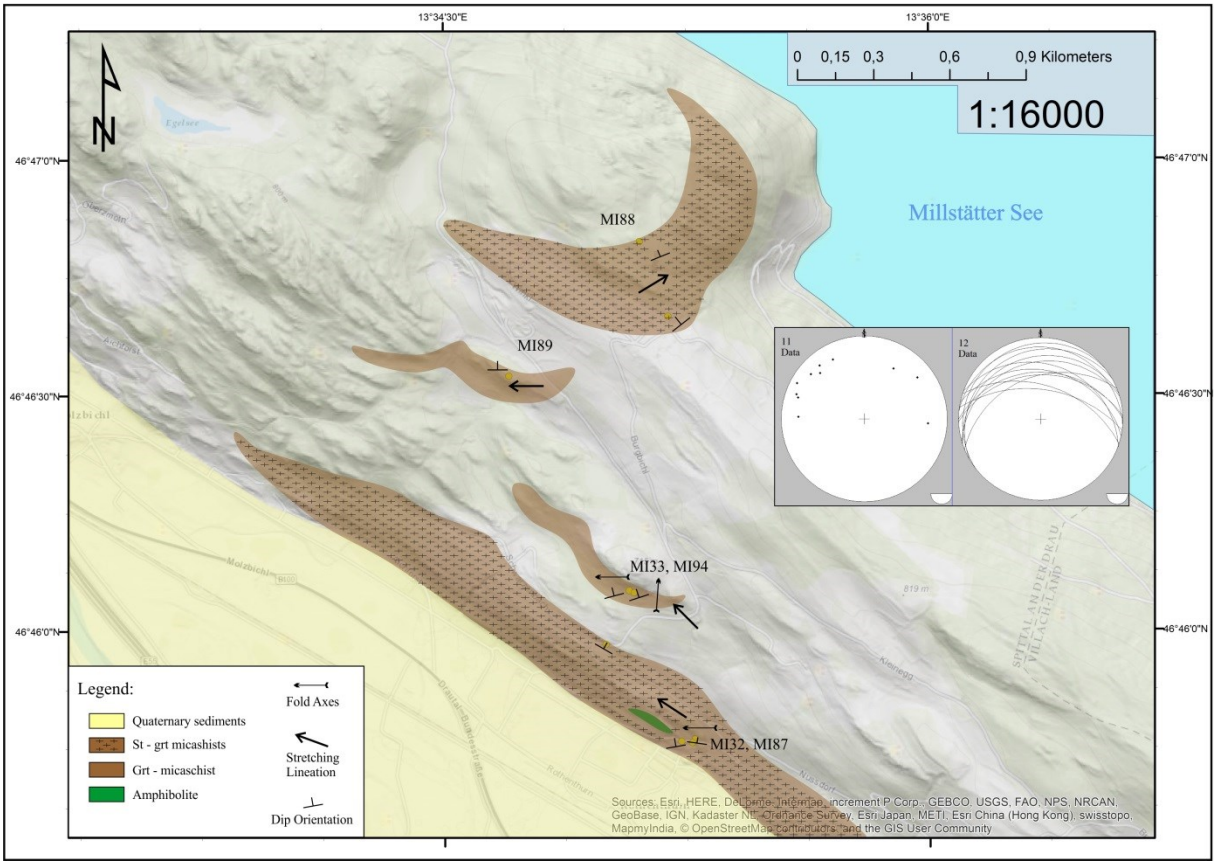

Fig. 8| Geological and structural map from area A, located at the Millstätter Seenrücken. Overlay downloaded from KAGIS.

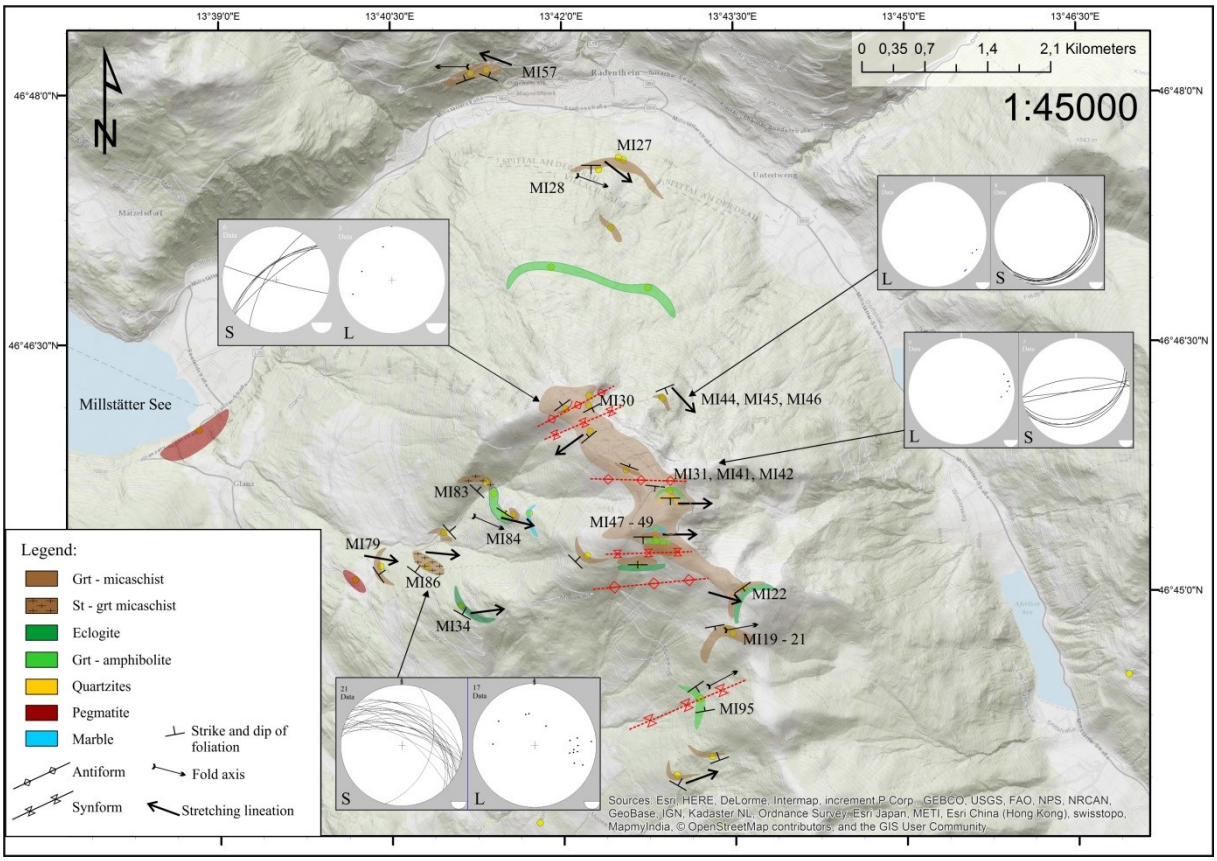

Fig. 9| Geological and structural map from area B

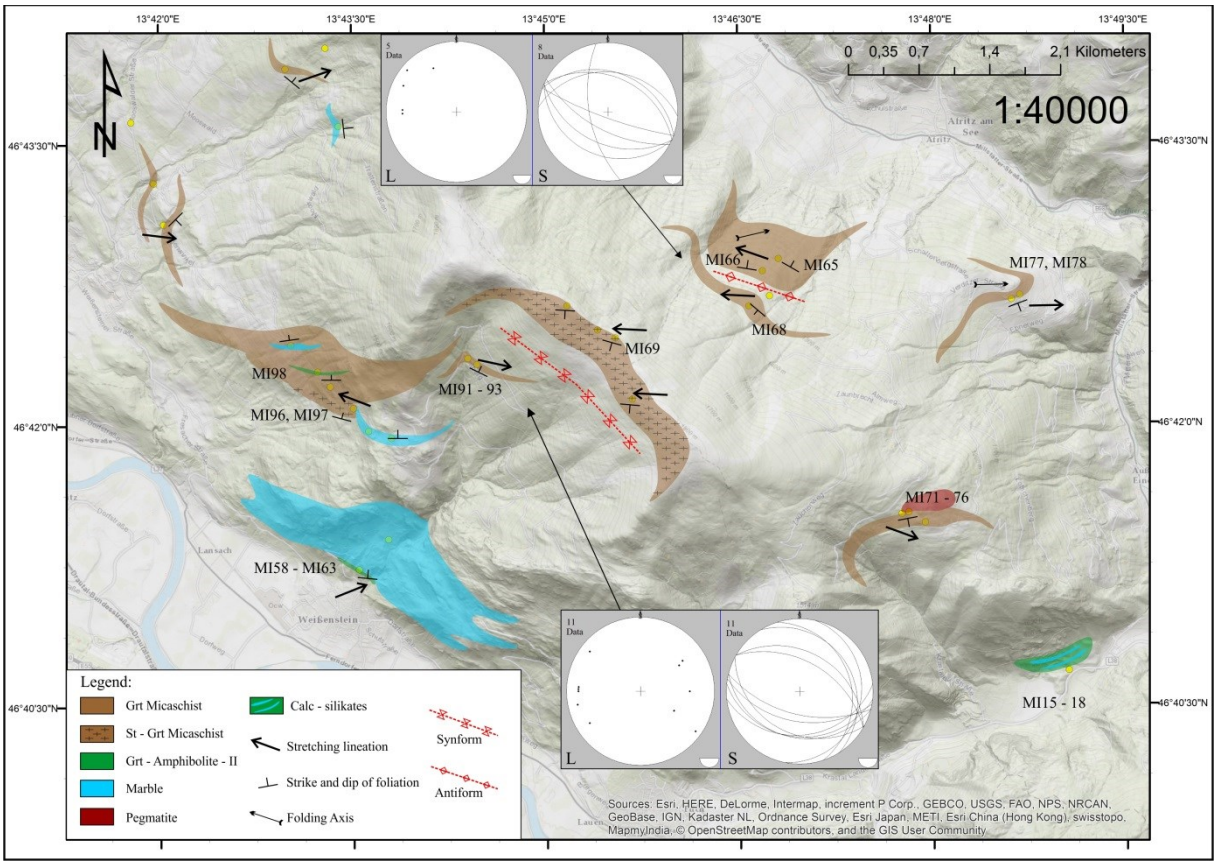

Fig. 10| Geological and structural map from area C

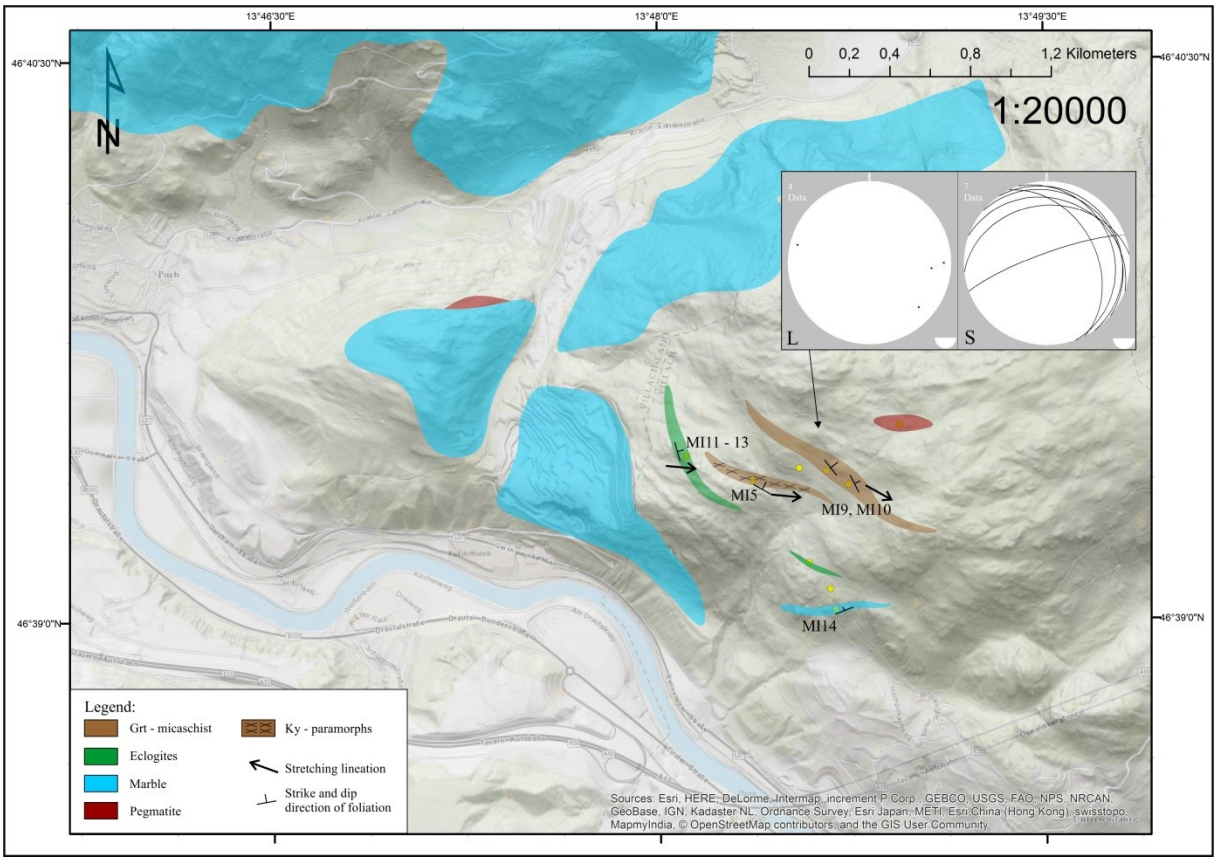

Fig. 11| Structural map from area D; Marble outcrops added from KAGIS GÖK-overlay.

Overall Structural Map:

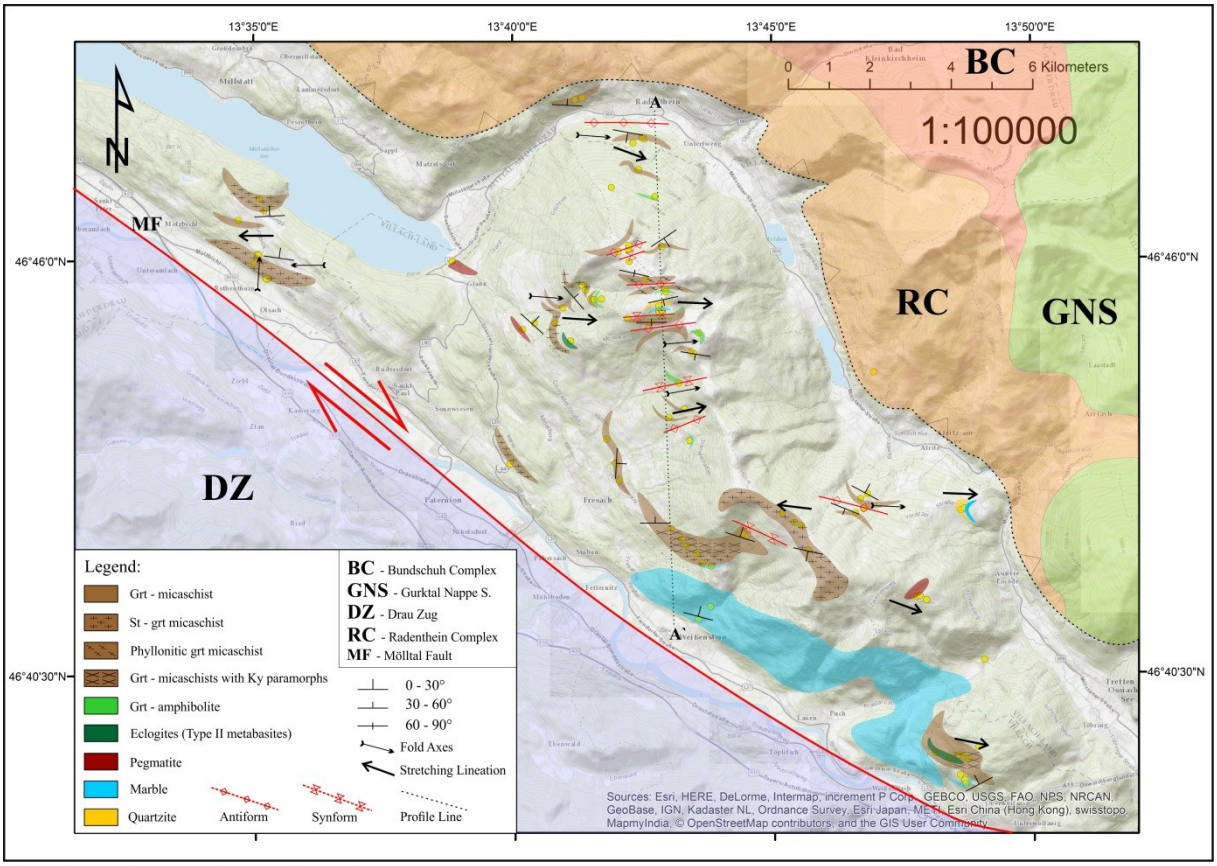

Fig. 12| Overall structural map of the study area.

Within figure 12, the most indicative structural data are displayed. They show a predominantly E-dipping stretching lineation in line with fold axes orientation, and planes dipping mostly to the SW as well as to the NE. From small outcrops in the field a major fold structure dominating the internal architecture of the MC was elaborated. The fold structure is SSW-vergent, and most of the central area is occupied by a large-scale M-shape fold structure.

The northern limb of the fold structure dips to the NNE, as shown by outcrops at the Millstätter Seerücken and north of the village Radenthein. In addition, previous mapping of the area, (carried out by the Austrian Geological Survey, GBA) display the contact between the MC and RC to be NNE-dipping.

Outcrops located near Glanz show st-grt micaschists and grt-micaschists with foliation dipping flat to ENE and E. These represent outcrops located near the hinge of the structure. There the measured foliation plane is interpreted as the fold hinge surface plane and its dip direction is almost comparable to the plunge angle direction of the fold axes representative for the major fold structure that dips flat to the E.

Data from the outcrops SE of the Mirnock summit show steep dipping grt-micaschists, which can be attributed to the inverse limb of the fold structure. Here the fold layer surface planes dip steeper than the foliation planes. Near the village Fresach, fold layer surface planes dip to the E, representing a further fold hinge area within the MC. Data near the Palnock summit reveal a upright limb with foliation planes dipping steeper than the fold layer surfaces.

From field mapping and structural observations a tectonostratigraphic profile was reconstructed (Fig. 13).

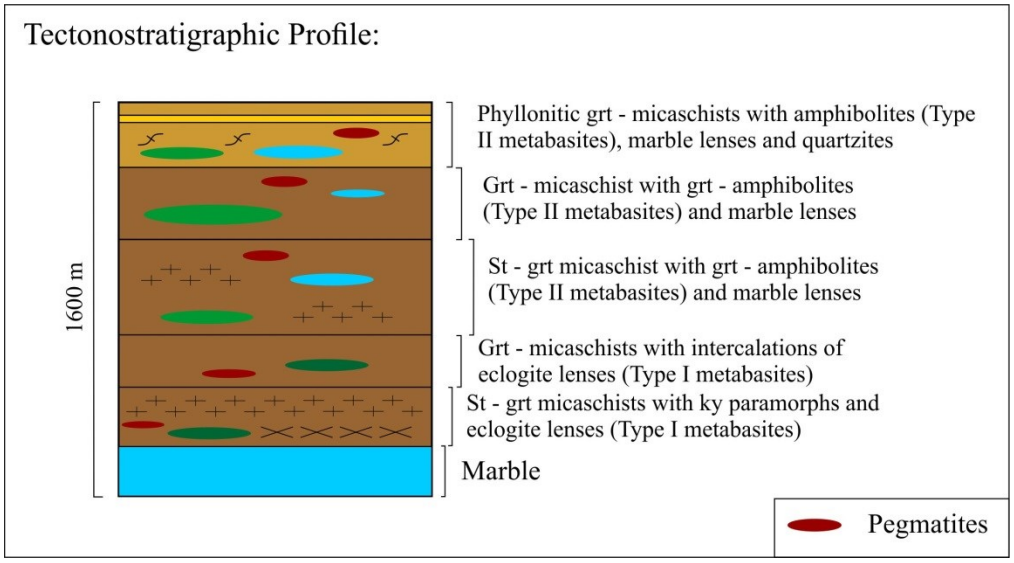

Fig. 13| Schematic tectonostratigraphic profile across the lithologies within the study area.

3.3 Profile

In order to reconstruct the internal structure of the MC, a geological profile has been created. The profile was selected to pass over the Mirnock (2110m) from Radenthein in the N to Weißenstein in the S (Fig. 14).

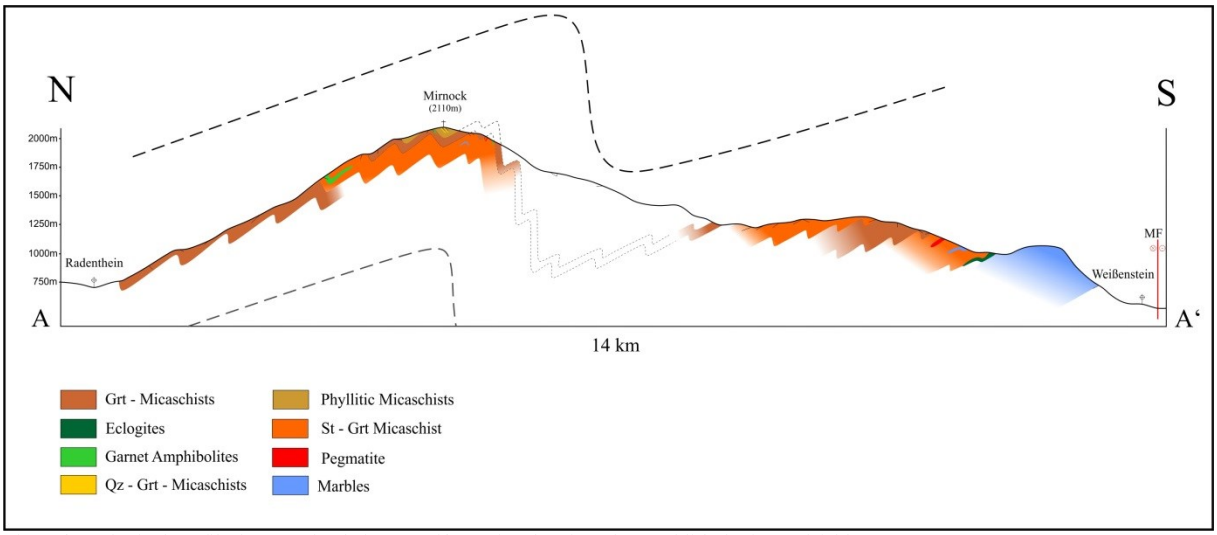

Fig. 14| Geological profile from Radenthein to Weißenstein, showing observed lithologies and fold structures.

4. Petrography

The petrological and microstructural analyses were obtained with transmitted polarized light microscopy. Based on field observations and petrographic investigations, major lithologies are classified as marbles, micaschists, and amphibolites.

Sample locations:

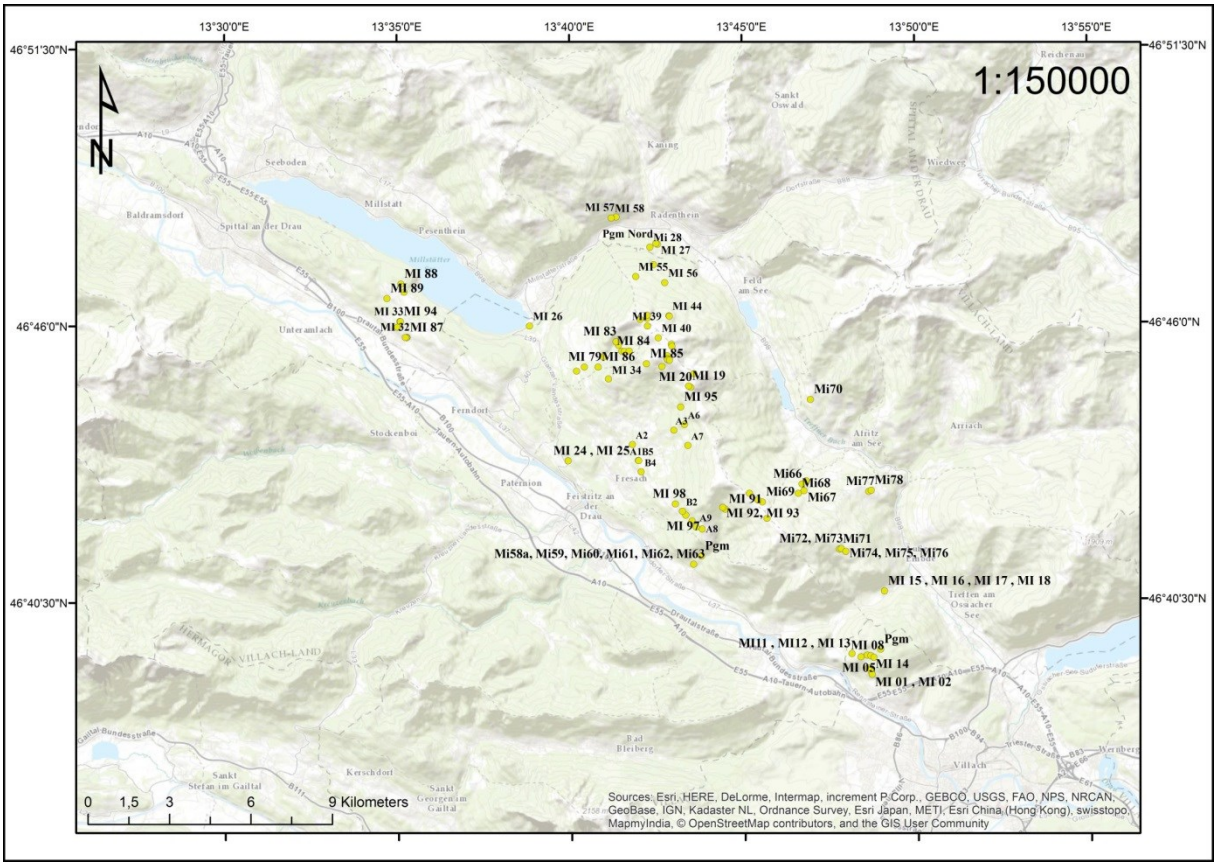

Fig. 15| Topographic map showing sample locations using GPS.

4.1 Metapelites

The micaschists of the MC represent the dominant lithology. Their subdivision within the MC is primarily based on characterizing mineral assemblages. From footwall to hanging wall, the following types of garnet - micaschists can be distinguished:

Type 1 Staurolite - garnet – micaschists

The typical mineral assemblage of staurolite - garnet micaschists consists of quartz + biotite + muscovite + garnet + kyanite + staurolite + plagioclase + tourmaline, accessory apatite and Fe-Ti oxides. Within the staurolite - garnet micaschists at the footwall, a higher abundance of biotite as well as fine-grained muscovite - garnet nests are observed (Fig. 16 a).

Staurolite occurs in two textural types: (i) large (up to 5mm) St I crystals, showing cracks and inclusions of quartz (Fig. 16 b), (ii) smaller St II (1 - 0.5mm) crystals with no inclusions (Fig. 16 c).

A few muscovite - garnet accumulations are characterized by the presence of relictic staurolite (St I; Fig. 16 d) fragments. Considering this retrograde textural observations, the following staurolite breakdown reaction towards hangingwall units is observed and explained by **staurolite I + biotite + quartz = garnet + muscovite + H_2O** (Spear, 1993).

Kyanite occurs as large grains (up to 1 mm) as well as in fine-grained nests (Figs. 16 d and e). Kyanite nests trace the shape of an older grain, most likely andalusite, and thus may represent paramorphic replacement of kyanite after andalusite (Fig. 16 e).

Garnet grains are observed in two textural types: (i) garnet crystals with inclusion-rich cores (quartz) and inclusion-free rims, from 0.2 to 4mm in size (Grt I, Fig. 16 c); (ii) hybidiomorphic, inclusion free garnets, from 1 to 3mm in size, with no visible zonation and resorption to biotite and chlorite (Grt II; Fig. 16 f). Grt I crystals are the most occurring type.

Type 2 Garnet – micaschists

Garnet – micaschists are mineralogically very similar to staurolite - garnet micaschists (Fig. 8 f). St I and II minerals are not observed. Kyanite paramorphs and textural occurrence of both micas are comparable to above described Type I micaschists.

Type 3 Phyllonitic garnet - micaschists

Phyllonitic micaschists occur within the hangingwall units of the MC. They are characterized by a higher abundance of muscovite and lesser quartz. Grt II contains no inclusions as well as retrogression. Some rims of these garnet crystals are chloritized and have chlorite-filled fractures. Associated quartzite layers range from dm to m in thickness. They contain small muscovite and garnet (Grt II) grains in the matrix.

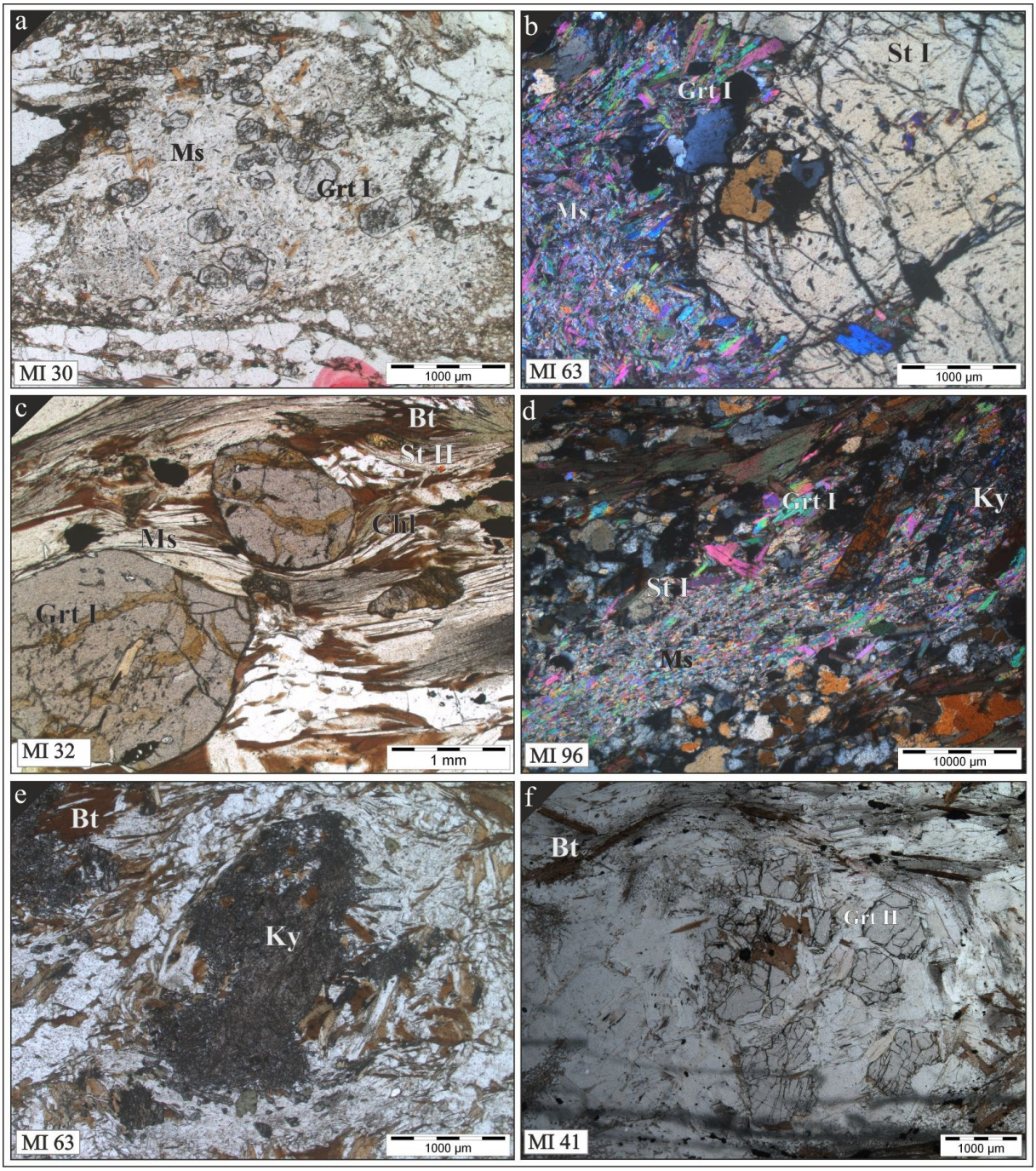

Fig. 16| **a)** Photomicrograph showing muscovite and Grt I accumulation within hangingwall garnet - micaschists; **b)** St I grain showing breakdown reaction to muscovite and Grt I at the rim **c)** Photomicrograph from sample MI32 with Grt I minerals and St II grains in the matrix; **d)** Muscovite + Grt I accumulation with residuary St I and kyanite; **e)** Thin section photomicrograph showing a kyanite after andalusite paramorphic replacement; **f)** Photomicrograph showing Grt II crystals in phyllonitic garnet micaschists.

4.2 Metabasites

Amphibolite lenses are found throughout the MC. Lenses located in the hangingwall differ in grain size, mineral assemblage and deformation. Variation in thickness is between 5 to 100m. Based on field relationships and petrographic investigations, two different types of metabasites have been identified (Type I and Type II):

Type 1: Eclogites

Relics of eclogites are only preserved within the southeastern MC, as boudins and thin layers (Figs. 17 a and b). In these rocks, Teiml (1996) described omphacite in light coloured layers, pointing to eclogite facies conditions.

Most of the Type I metabasites are retrogressed to garnet-bearing amphibolites (Samples: MI3, MI34; Fig. 17c) and characterized by the mineral assemblage quartz + garnet + amphibole + plagioclase + diopside + epidote + accessoric titanite, zircon, Fe-Ti oxides and calcite. Garnets occur in two textural types: garnets up to 5 mm in size, containing inclusions of quartz (Fig. 17c) and smaller (from 0.5 to 2 mm) garnets showing strong resorbtion into greenish keliphitic rims due to the retrograde reaction: **omphacite + garnet + H_2O = amphibole + $Mg_{-1}Si_{-1}Al_2$** (Hoinkes et al., 1991) (Fig. 17 d).

Due to the symplectitic intergrowths of diopside, plagioclase and amphibole (Fig. 17c), retrogressed Type I amphibolites represent former eclogites (omphacite = clinopyroxene + plagioclase + amphibole + quartz). Teiml (1996) described rocks from this eclogite unit as a paragenesis of quartz + garnet + omphacite + amphibole + phengite + epidote + clinozoisite + rutile + ilmenite and calculated a P/T range between 12 – 14 kbar and 650 – 680 °C, using albite – jadeite - quartz barometry and garnet - amphibole thermometry.

Type 2: Garnet-amphibolites

Garnet-amphibolites towards the hangingwall of the complex show no symplectitic textures. The garnets are small and show frequently almost complete resorption into biotite + plagioclase. Therefore they experienced lower peak metamorphic grades compared to Type 1 eclogites at the footwall. In addition they have smaller grain sizes and an alternating layering between amphibole-rich and plagioclase-rich layers (Fig. 17 e).

The paragenesis differs slightly from Type I metabasites, mainly consisting of: amphibole + quartz + garnet + plagioclase + epidote + clinozoisite + calcite + paragonite. Calcite and biotite are subordinate phases. Amphibolites with calcitic layers and paragonite are also attributed to this lithology, but occur only as thin layers associated with classic amphibolites (Fig. 17f). Locally they can be referred to as paragonite-amphibolites (MI22) and metamorphic calcsilicate rocks (MI16-18).

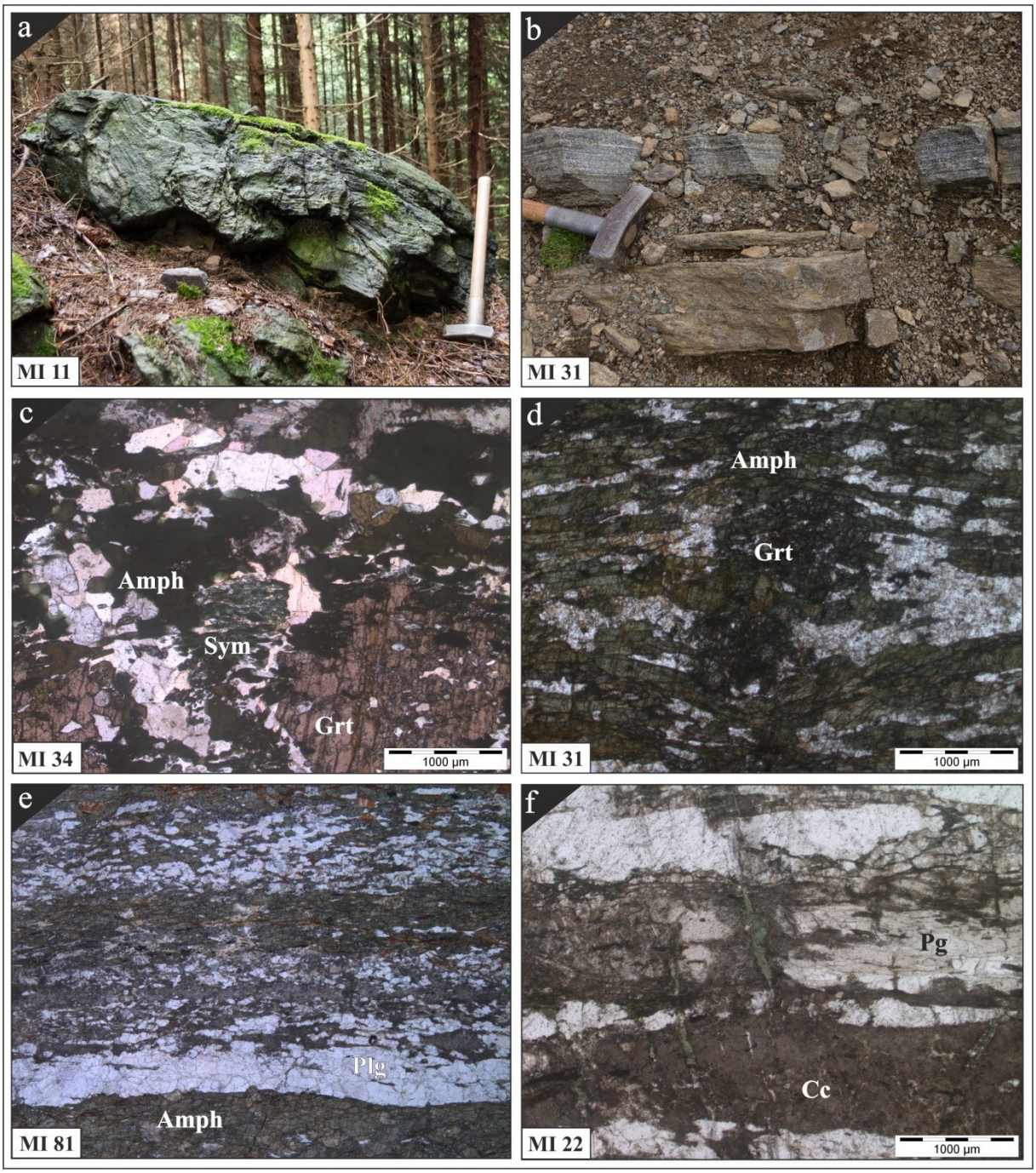

Fig. 17| **a)** Amphibolite-boudin outcrop from the Wollanigberg; **b)** Thin amphibolite outcrop near the Mirnock summit; **c)** Thin section photomicrograph from a retrogressed Type I eclogite showing garnets and symplectite textures; **d)** Resorbed garnets in Type 2 amphibolite; **e)** Alternating layers of plagioclase - and amphibolite -rich zones in Type 2 amphibolite; **f)** Type 2 amphibolite with high content of paragonite (Pg) and Calcite (Cc).

4.3 Metacarbonates

Within the footwall units of the MC, tremolite-bearing marbles occurs. At the southeastern end this unit forms several 100m thick outcrops (Fig. 18 a). Towards the hanging wall, however, the marbles thin out (several 10 m) (Fig. 18 b). The largest occurrence is near the village Puch where marbles quarries occur.

Marble is in general coarse-grained with elongated tremolite crystals (several cm in size) visible at macroscopic scale (Fig. 18 b). The main mineral assemblage is calcite + dolomite + tremolite ± diopside ± talc and quartz. These rocks are almost pure calcite marbles (Fig. 18 c and d) and have stratigraphic ages from Late Silurian to Lower Devonian (Puhr, 2009). Tremolite shows strong alterations (Fig. 18 e) and formed due to a retrogressive reaction from diopside, defining amphibolite facies metamorphism of metacarbonates (**5 diopside + 3 CO_2 + H_2O = tremolite + 3 calcite + 2 quartz**; Spear, 1993). Further retrogressive reactions of tremolite can form talc (**tremolite + dolomite + CO_2 + H_2O = 2 talc + 3 calcite**; Spear, 1993). Accessory phases include rutile, pyrite, pyrrhotine and chalcopyrite.

Fig. 18| **a)** Quarry near Puch; **b)** Marble sample collected near the Mirnock, showing tremolite minerals; **c)** and **d)** Photomicrograph from Sample MI14, near the Wollanigberg; **e)** Thin section containing altered tremolite and relictic diopside.

5. Macrostructures

5.1 Structures within micaschists

Garnet-micaschists show an overall SE- and NNW-dip direction. Measured stretching lineation data plunges flat to the E (Fig. 19 a) following b axis. This is explained by the fold plane schistosity crosscutting with the fold surface planes. WNW oriented linear features are visible locally and can be attributed to an earlier stretching lineation L_1. From larger outcrops fold structures are observed where limbs dip flat to SSE and steep to N or S. Fold axes plunge generally flat to E for the whole unit. These larger fold structures are representative for the central areas of the complex, exposed at higher structural levels, near the Mirnock and Palnock summits.

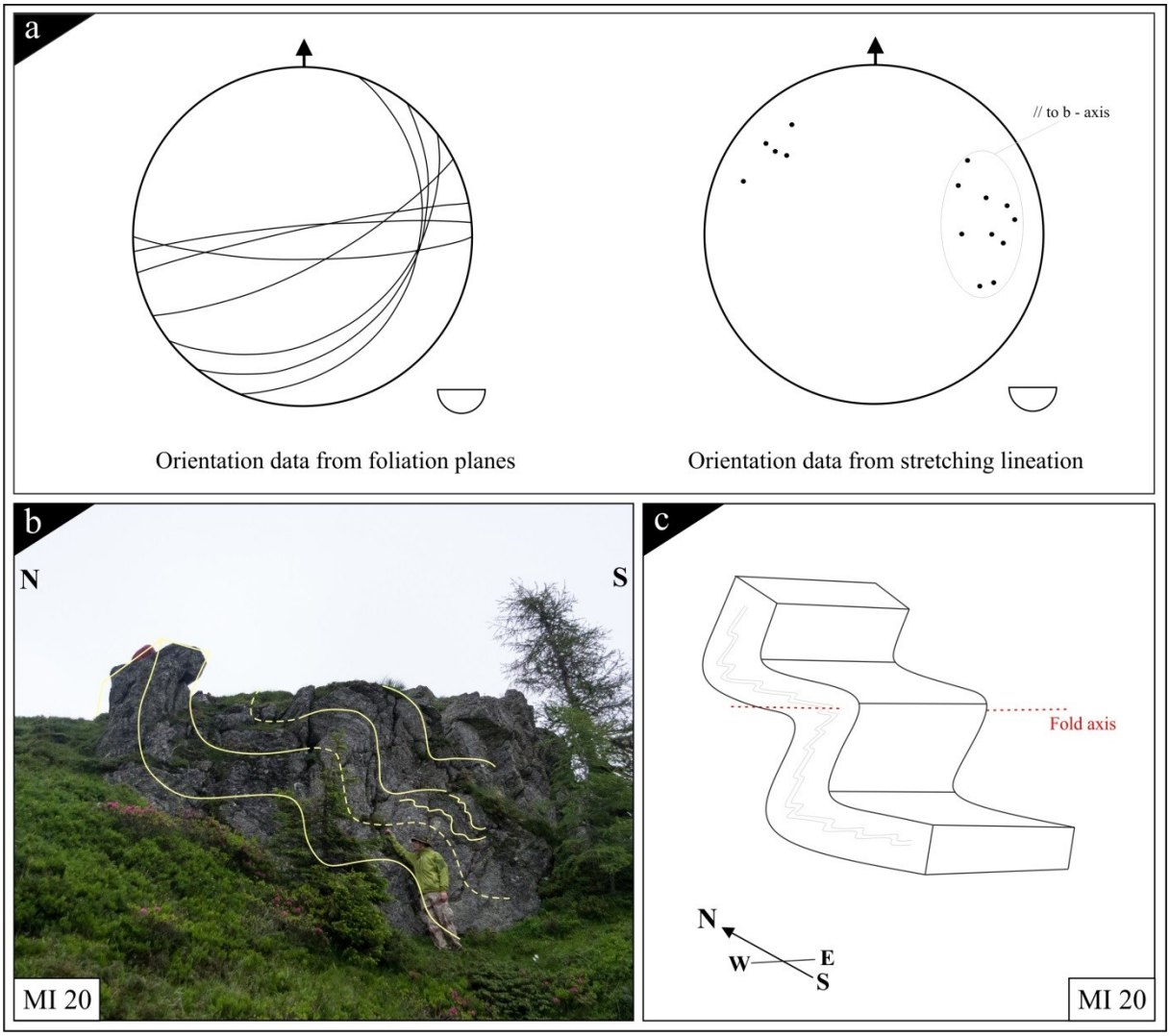

Fig.19| **a)** Stereo plot of foliation and stretching lineation data. Foliation planes represent fold - limbs; **b)** Micaschist outcrop at the center of the MC showing representative fold structure; **c)** Schematic fold structure from MI20 with flat-to-the-E plunging fold-axes.

Macroscopic structures are visible within most outcrops. Grt-micaschists show well foliated samples and symmetric pressure shadows around garnets and feldspar minerals, most likely developed along with flattening deformation (Fig. 20 a). Asymmetric folded S_1 foliation planes occur in the XZ structural planes, also indicating flattening deformation (Fig. 20 b).

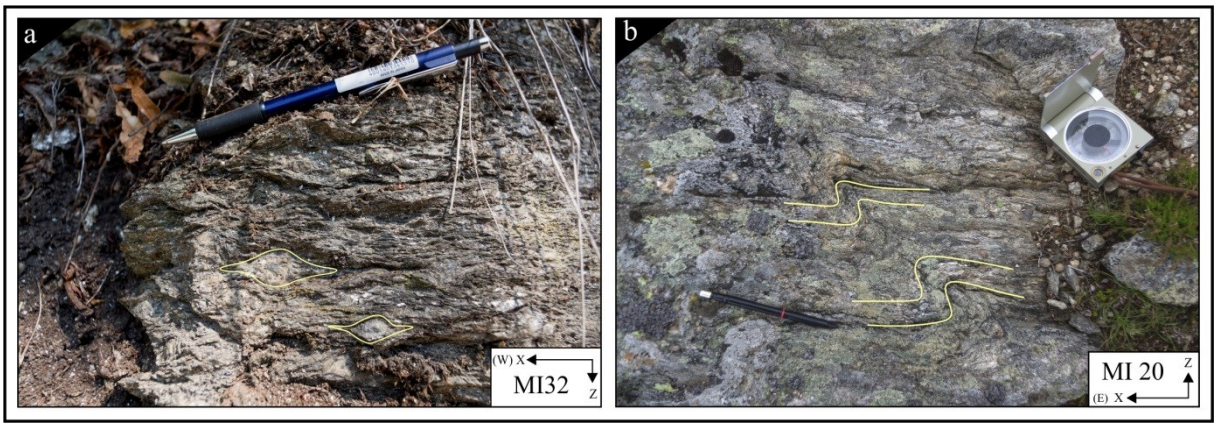

Fig. 20| Photographs of macrostructures; **a)** Symmetric pressure shadows around feldspar minerals, within footwall st - grt micaschists in study area A; **b)** Asymmetric tight folds F_1 within grt-micaschists in study area B.

5.2 Structures within amphibolites

Macro-scale structures are predominantly visible in Type II metabasites and characterize an intense foliation with alternating plagioclase-rich layers and dark amphibole-rich layers.

Figure 21 (a) summarizes measured orientation data. Tight folding of S_1 structural planes results into almost isoclinal folds F_2 (Figs. 21b and c). These fold structures are surrounded by a subsequent developed schistosity S_2, which evolved during exhumation of the eo-Alpine wedge.

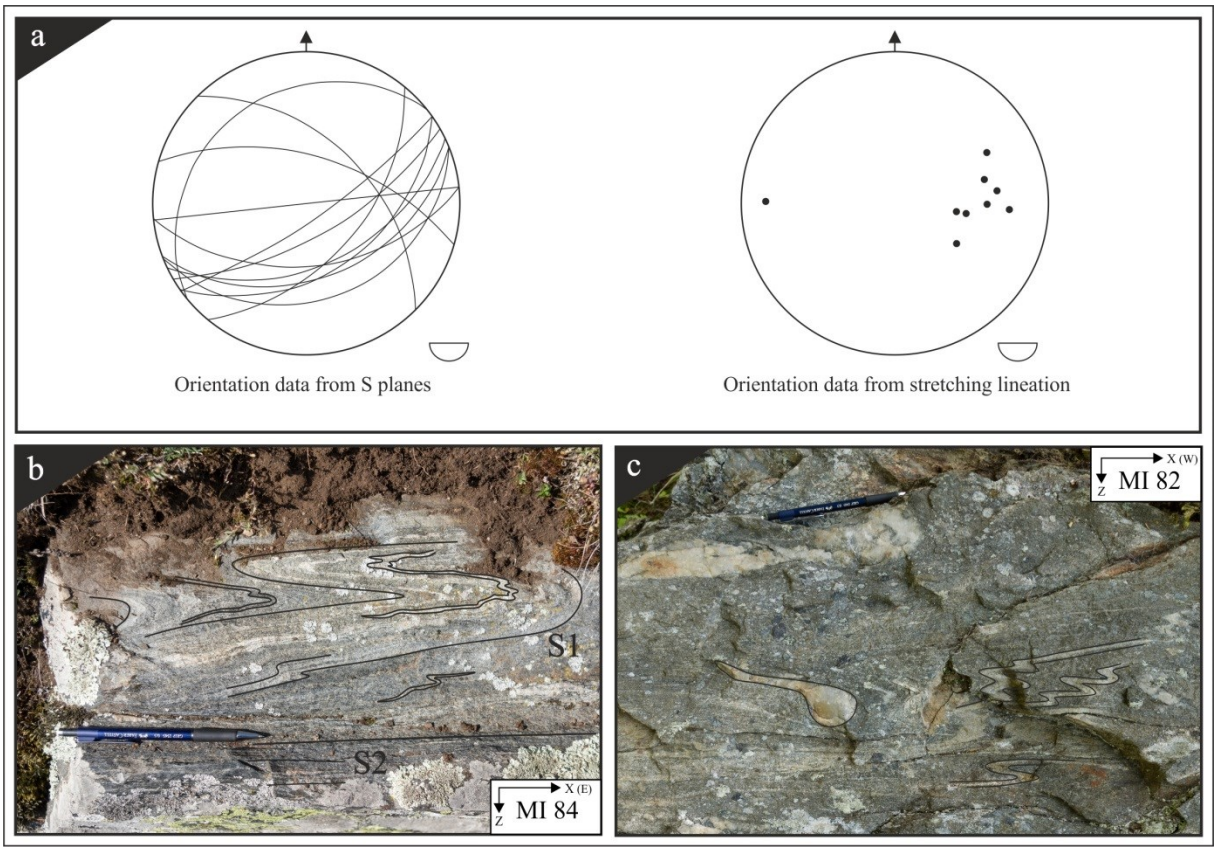

Fig.21| **a)** Plot of measured S-planes and stretching lineation in amphibolites; **b)** MI84 outcrop displaying older internal fold structure F_1 in contrast to a discrete schistosity S_2; **c)** MI82 outcrop showing closed folding F_1.

5.3 Structures within Marbles

The marbles within the MC dip generally to the N and indicate locally thrusting and subsequent brittle deformation overprintings (Fig. 22 a and b). The coarse-grained rocks show fold structures, with E-dipping fold axes, which are cut by younger SE-dipping normal faults. The fold structure may be linked with NW directed nappe stacking (D_1; early Cretaceous). Related stretching lineation L_1 plunges shallowly to the SE. Late Cretaceous brittle deformation crosscuts fold structures and is interpreted as extensional normal faulting following the eo-Alpine nappe stacking event (Fig. 22 b).

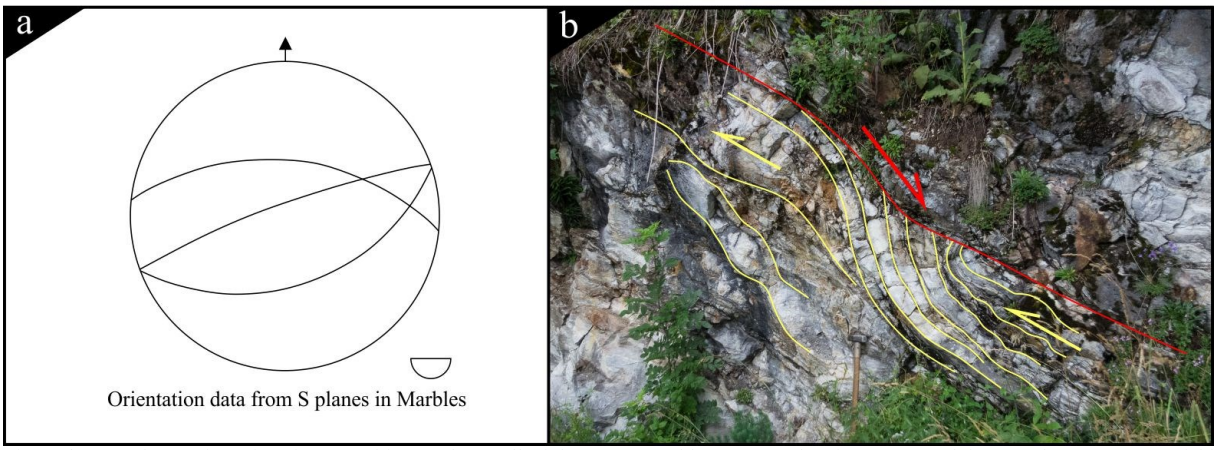

Fig. 22| **a)** S-plane orientation from marbles at the Wollanigberg; **b)** Marble outcrop showing D1 eo-Alpine (Early Cretaceous) fold structures (yellow) and Late Cretaceous extensional brittle deformation (red).

6. Microstructures

Oriented samples were collected and cut parallel to the stretching lineation direction (X) and normal to foliation (Z) to obtain informations for intracrystalline deformation mechanisms and shear sense directions.

Micaschists show a well-developed foliation throughout the MC. The microstructures include garnet porphyroblasts, microlithons and lesser developed SC-planes. However, a high degree in flattening deformation dominates in the MC. SC-planes, if present, can be ambiguous in one sample and not ideal for interpretation (Fig. 23 a).

In staurolite - garnet micaschists Grt I porphyroblasts show synkinematic growth patterns, recording an early foliation S_0 within the core (Fig. 23 b), as well as symmetric pressure shadows, indicative for a later deformation overprint D_2 by dominant pure shear deformation (Fig. 23 c). Microfolds within garnet micaschists characterize an early deformation with respect to field foliation S_2 (microlithons in Fig. 23 d).

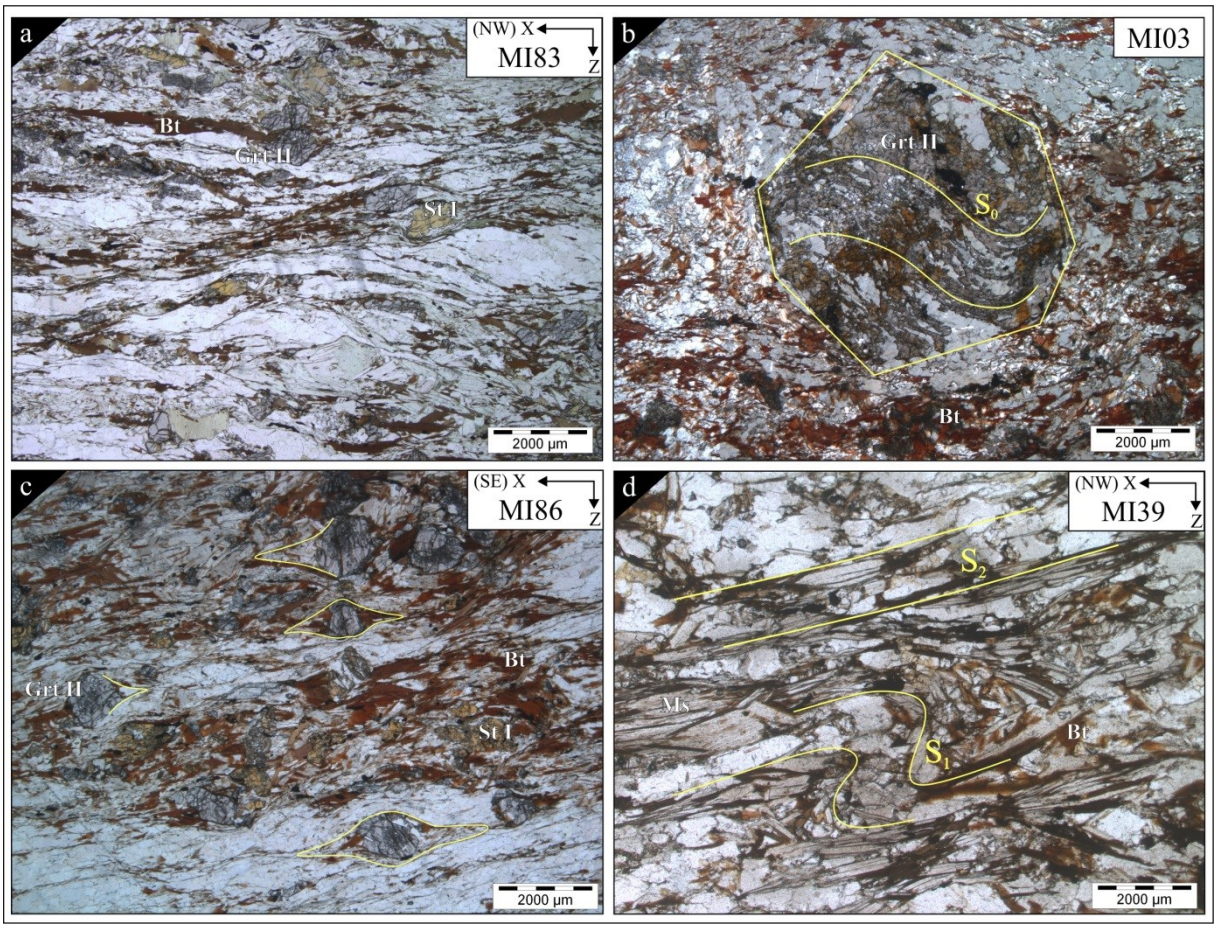

Fig. 23| Photomicrographs from thin sections; **a)** St-grt micaschist with showing ambiguous SC structures; **b)** Synkinematic Grt I, showing internal S_0 foliation, near the Wollanigberg; **c)** St-grt micaschist showing grt-porphyroblasts with symmetric D_2 pressure shadows; **d)** SE-vergent microlithons in phyllonitic micaschists and S_2 field foliation.

7. Structural evolution

Available observations have been used to reconstruct a tectonometamorphic evolution of the Millstatt Complex.

After Schuster (2004), there is no evidence for a Variscan metamorphic event within the KWNS. Therefore the primary mineral assemblage was generated during Permian high temperature/low pressure metamorphism, associated with formation of Grt I cores, St I and andalusite. Pegmatite intrusions are wide spread across the unit and are also linked to this event.

D_1 structures in the MC are represented by synkinematic Grt I growth, incorporating an older schistosity S_0. Shearing and folding during this early stage, leads also to the development of D_1 structures including S_1, L_1 and F_1. They developed during the early exhumation stage. This non-coaxial deformation stage was followed by coaxial strain resulting into the formation of large scale fold structures F_2 and associated S_2 field foliation. (Figs. 20 a/b and 21 b/c).

In Late Eocene, Early Oligocene times, along with the indentation of the Apulian microplate, the major re-orientation of the eo-Alpine structures took place. Large scale F_2 folds were tilted into the present day SSW-vergent large-scale fold structure, with flat to the east plunging fold axes (Fig. 14 and 19 c). This results into high variable dip directions between the S_2 foliation and the associated F_2 fold plane surfaces.

8. Major element garnet profiles

Polished thin sections were analyzed with a scanning electron microscope JEOL JSM-6310, attached to a wavelength dispersive system with an acceleration voltage of 15kV, at the University of Graz, Institute of Earth Sciences, Department of Mineralogy and Petrology. The obtained data is displayed in the following major element profiles across the studied garnet generations.

Garnets from different locations (Fig. 25) show generally a high X_{alm} component (from 0.7 to 0.8) and continuous major element zonation patterns are primarily visible in X_{alm}, X_{grs} contents. The patterns obtained can be divided into two groups, which are described in the following.

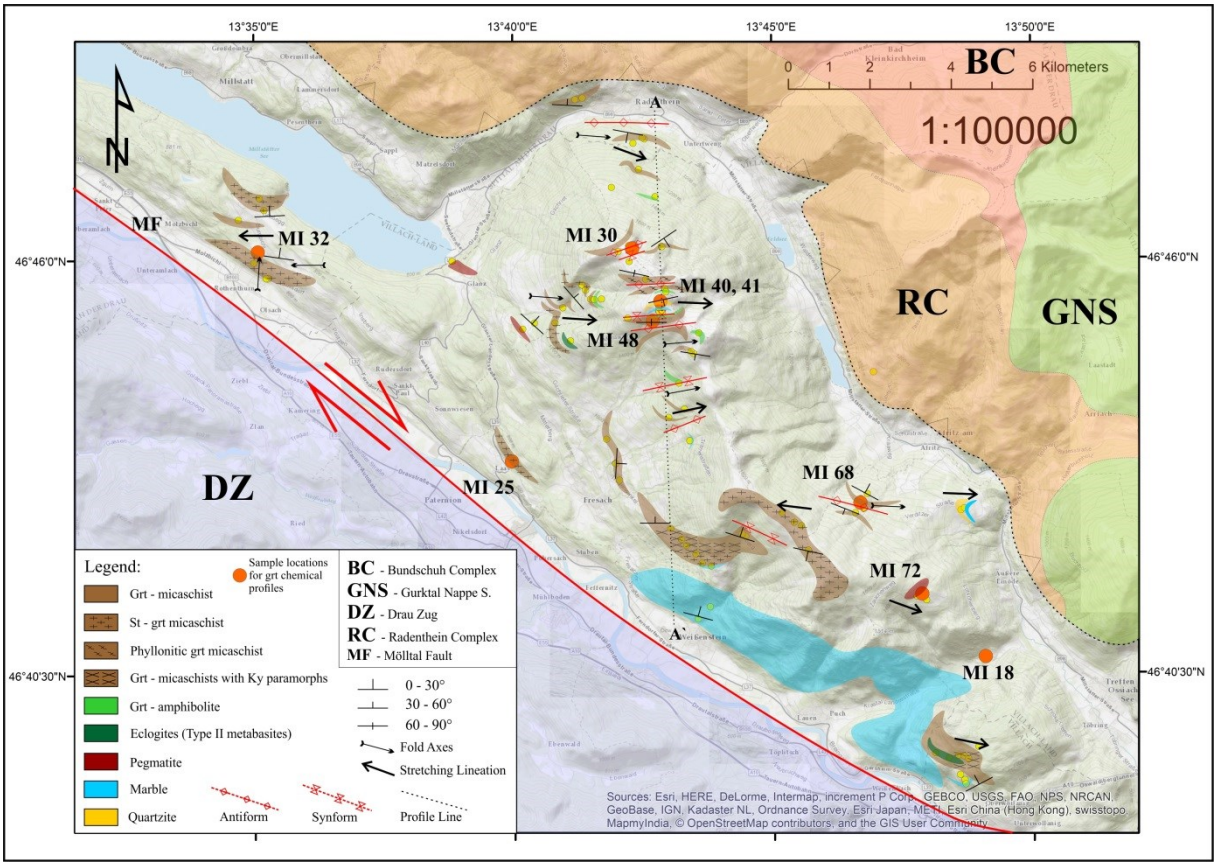

Fig. 25| Map showing location of selected garnet samples in their respective lithological framework.

Type A garnet profiles

Garnet profile patterns from type A show a continuous, monometamorphic, chemical zonation. Sample MI40 from phyllonitic micaschists at hangingwall units of the MC represents garnets (Grt II) with a zonation pattern, indicative for a single growth phase (Fig. 26 a). These rocks contain more muscovite, subordinate biotite and coarse grained quartzite layers. Garnets differ from Grt I grains in other samples in terms of far more less inclusions, retrogressive reactions and show no pressure shadows. X_{Sps} shows slightly increasing values at the outer rims, reflecting the retrogressive reaction during decreasing temperatures (Spear et al., 1993).

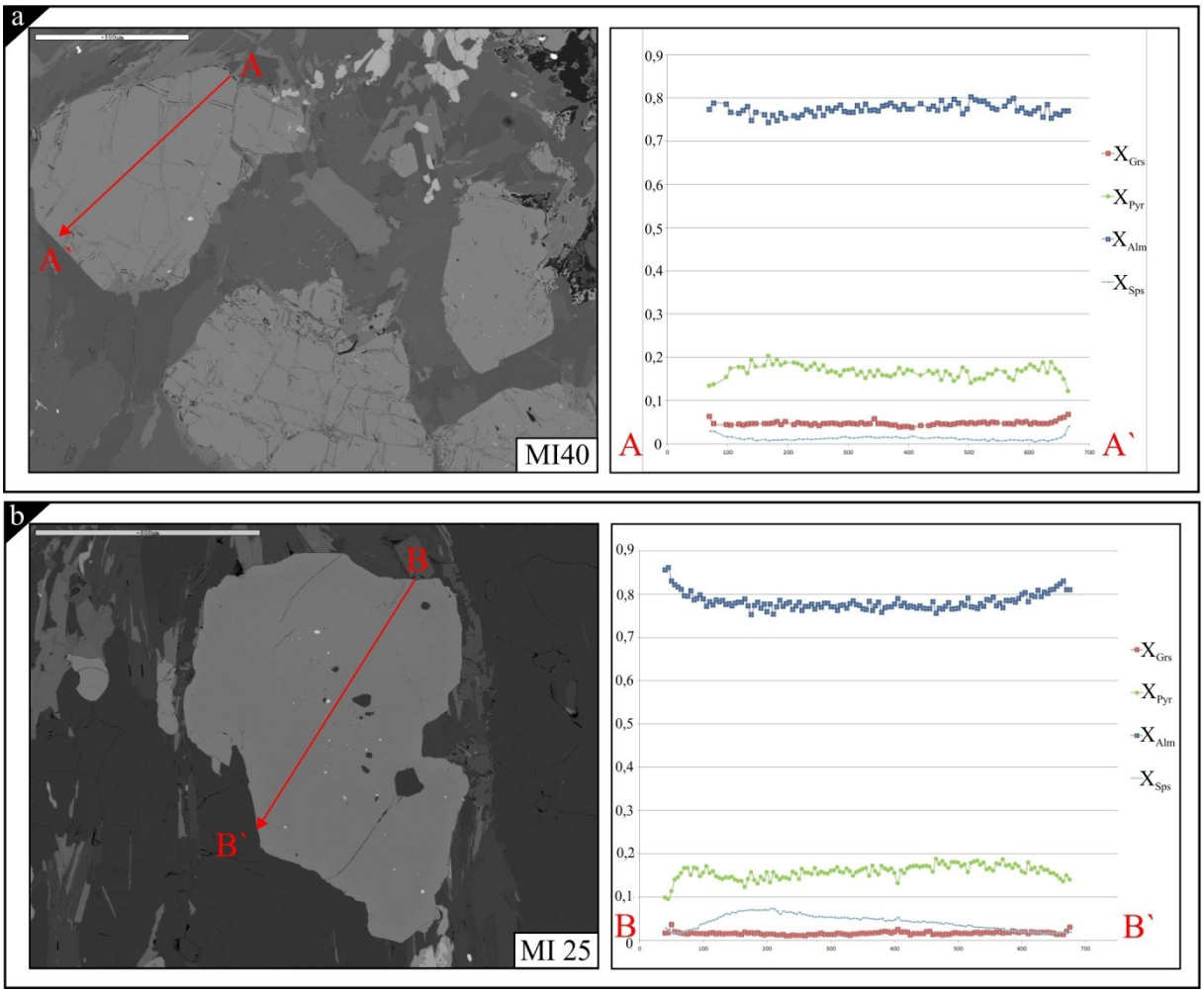

Fig. 26| **a)** Chemical zonation patterns from Grt II grains in sample MI40, at the Mirnock summit; **b)** Chemical zonation pattern from sample MI 25 from the south of the MC.

The chemical data in Fig. 26 b from sample MI25 shows a monometamorphic garnet (Grt I) with quartz inclusions. It shows a typical X_{Sps} bell-curve, which formed during the pro-grade path mostly related to the eo-Alpine metamorphic event.

Type B garnet profiles

Type B garnet profiles show continuous, monometamorphic zonation patterns. Sample MI41, from the Mirnock summit shows a Grt II chemical profile with higher X_{Grs} values in the core area, and an opposing trend for X_{Pyr} values (Fig. 27 a). X_{Sps} and X_{Alm} on the other hand show constant values. This pattern is interpreted to have begun to develop at almost peak-T conditions, reflecting a pressure decrease during its growth.

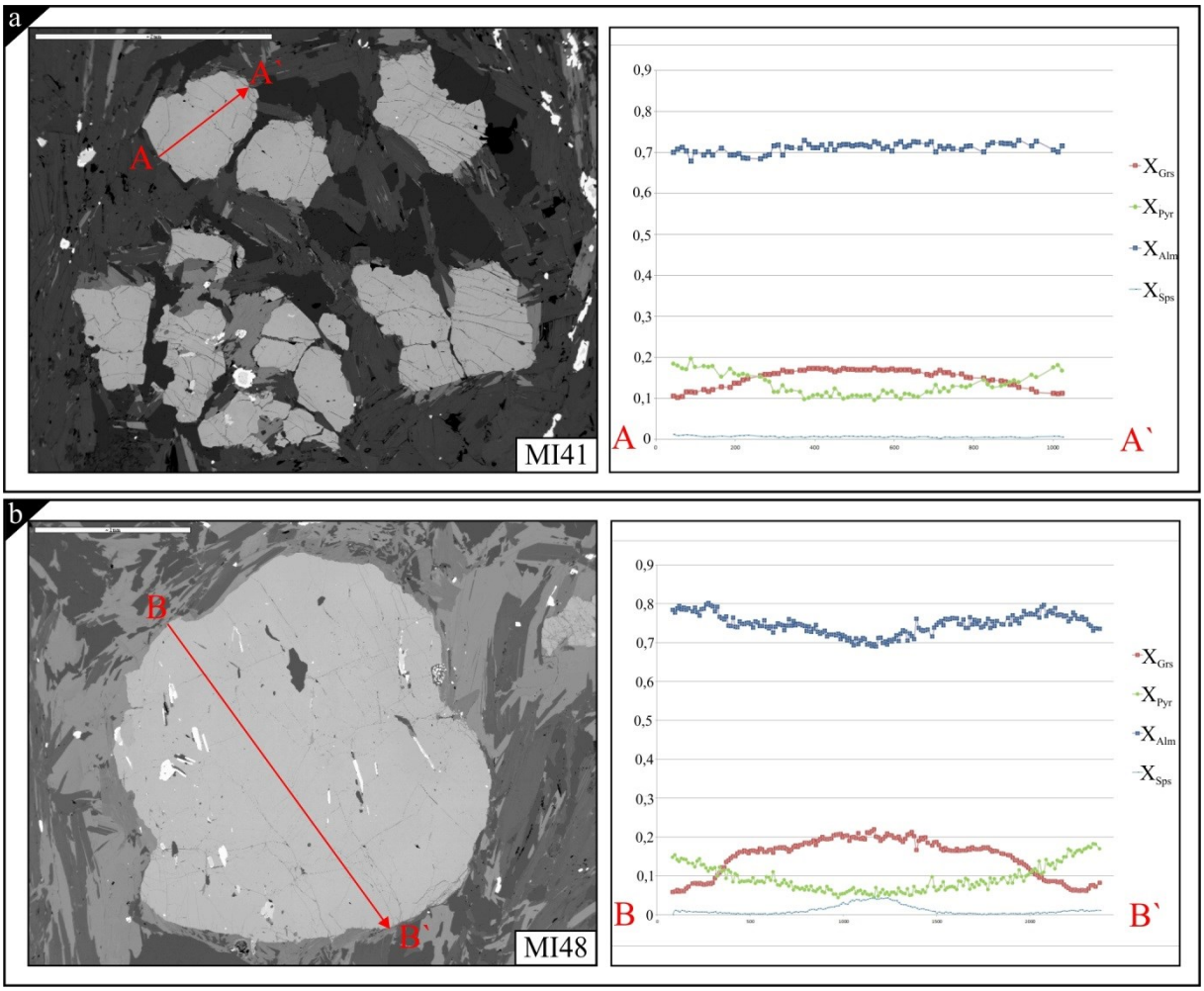

Fig. 27| **a)** Chemical profile from sample MI41, at the top of the MC with characteristic higher X_{Grs} at the core; **b)** Chemical profile from sample MI48, at the top of the MC, showing a bell-shaped Mn-chemical zonation pattern, as well as higher X_{Grs} values in the core.

Sample MI48, from most hangingwall units of the MC, is characterized by a prograde garnet core, visible in X_{Sps} values in the centre of the profile (Fig. 27 b). The chemical pattern is continuous. It is therefore monometamorphic, most likely to have grown during the eo-Alpine event at higher pressures towards peak T-conditions.

Type C garnet profiles

Type C garnet profiles show a characteristic zonation pattern. Cores show high X_{Grs} values whereas rims show lower values. This zonation type is referred to as the "Laas type".

Figure 28 shows a chemical profile across a Grt I mineral in sample MI32 from the "Millstätter Seerücken" at the base of the MC, from st-grt micaschists. The chemical pattern

shows the “Laas type” garnet zonation within the core, whereas the rims are characterized by a rise in X_{Grs} values.

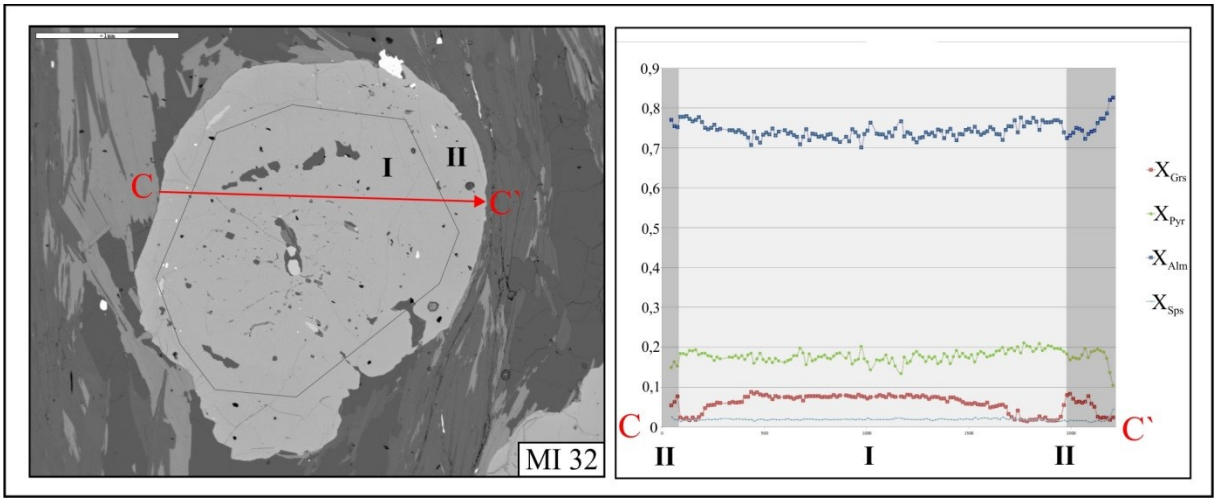

Fig. 28| Type B garnet profile from sample MI32, showing prograde growth in the core, and X_{grs} increase at the rims.

The increase in X_{Grs} values at the rims is most likely to have happened during the same growth phase, following changes in the bulk chemistry. In this sample, thin sections show the presence of St II minerals, which can also incorporate Ca in their structure. If the overall Ca concentration is poor within the bulk chemistry, then the simultaneous growth of St II would probably result in depletion of X_{Grs} values within garnet minerals.

In figure 29 a and b, chemical profiles from the same sample MI48 are shown. The sample occurs in hangingwall units of the MC, containing garnets with “Laas type” zonations. This zonation pattern has been observed within previous studies in the Schneeberg Complex (SC), as well as the Laas Unit (LU) west of the TW by Heinisch (2014) and Konzett (1990).

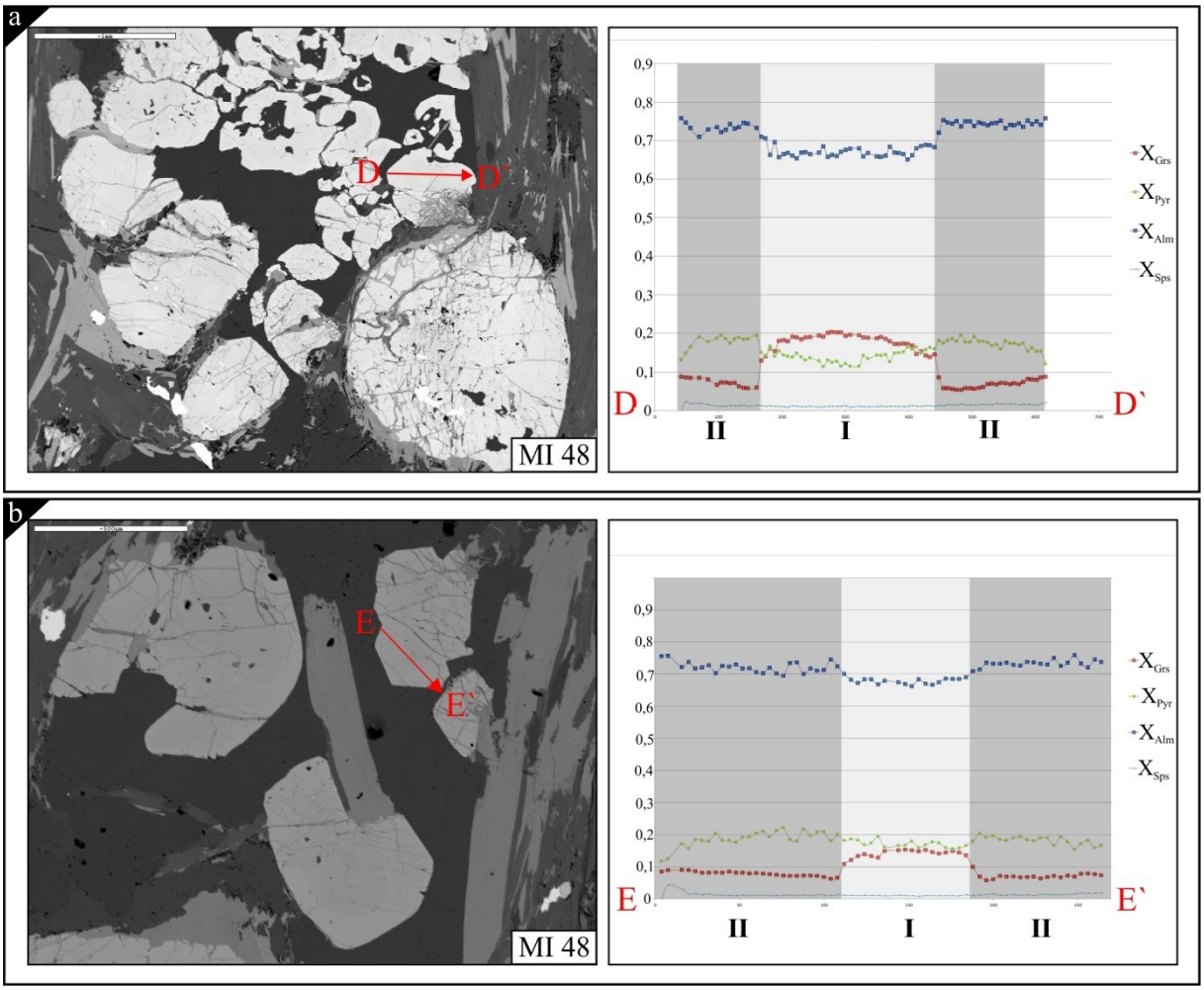

Fig. 29| BSE images and respective chemical profiles across garnets from sample MI48; **a)** garnet shows high X_{grs} content in the core, and lower in the rims; **b)** shows the same trend, but at overall lower values, and is less indicative for polyphaser garnet growth.

These garnets are not seen to have a polymetamorphic character, mainly because of the continuous nature of the chemical patterns, and because of the very constant X_{Sps} concentration across the minerals. The X_{Grs} value rises within the rims slightly indicating changes in the amount of free Ca in the system. This change may be caused by the staurolite I breakdown to garnet and muscovite during the eo-Alpine metamorphic event (Heinisch, 2014).

Garnets from such garnet and muscovite nests show inclusion-rich cores, and inclusion free rims (Fig. 30). The garnets most likely began to grow during the reaction of staurolite to muscovite and garnet, where less Ca was free in the system. As staurolite continues to break down, more Ca is available for the garnets to incorporate. The left hand side of the profile reflects the continuous increase of Ca in the system, also visible in figure 29 a and b, where Ca slowly increases towards the garnet rims.

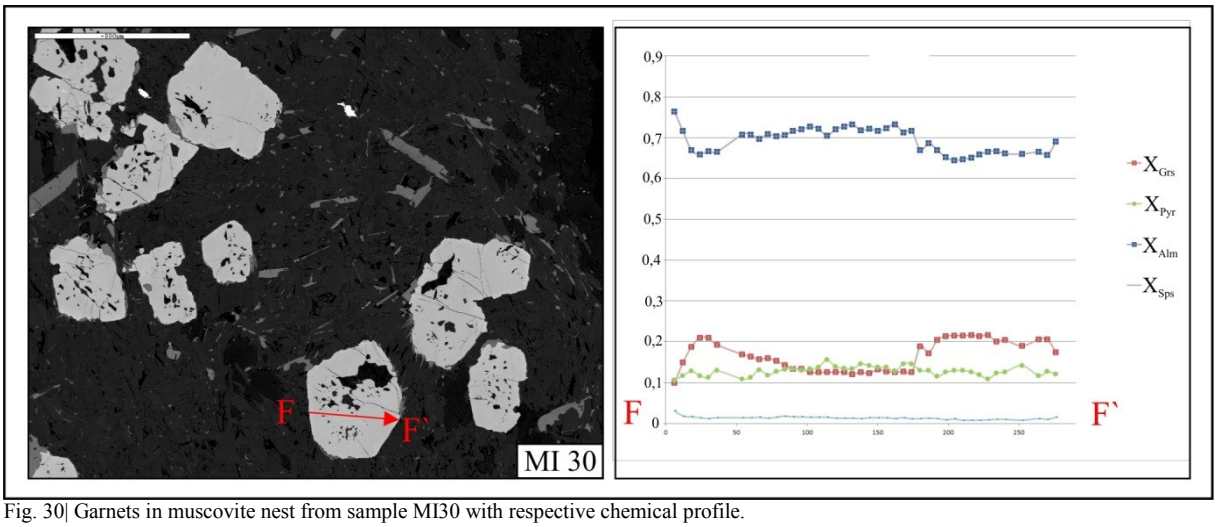

Fig. 30| Garnets in muscovite nest from sample MI30 with respective chemical profile.

9. Discussion

From studies about the KWNS, especially from the Koralm-Saualm unit, no evidence for a Variscan metamorphism is proposed, which supports our investigations from the MC. The Permian event however is well documented through Grt – core dating (Habler and Thöni, 2001) and Rb-Sr whole rock ages from pegmatites (Schuster and Frank, 1999). These observations correspond also to the MC, although no local age information is present. The Permian event within the MC leads amongst others to pegmatitic melts and primary metamorphic assemblages, which have been overprinted during the eo-Alpine metamorphic event. The main described structures (D_1/D_2) developed during the Early Cretaceous; there is no evidence for a former structural imprint.

The subsequent indentation of the Apulian microplate in Late Eocene times, resulted into intense N to S shortening within the Austroalpine, and with respect to the KWNS and its nappes structurally above, to re-orientation of the eo-Alpine structures (Figs. 19 b and c), finally characterized by a large-scale SSW-vergent fold structure which dominantes the internal architecture of the MC.

9.1. Comparisons to the units west of the Tauern Window

The Units of the Texel Complex (TC), Laas Unit (LU) and Schneeberg Complex (SC), west of the Tauern Window (TW) are also part of the KWNS. Prior to the unroofing of the TW the units west and east of the TW were merged and experienced therefore the same tectonometamorphic evolution during eo-Alpine times and earlier (Krenn et al., 2011; Frisch et al., 2000; Pomella et al., 2015).

The TC is an eclogite-bearing, polymetamorphic unit in the footwall of the LU that is defined as a polymetamorphic, marble- and pegmatite bearing unit (e.g. Hoinkes et al., 1999). The SC in the hangingwall of the LU characterizes a monometamorphic metasedimentary unit, comparable to the RC in the east of the TW (e.g. Krenn et al., 2011).

The MC and the TC have been compared and defined as one Austroalpine nappe unit, due to the presence of eo-Alpine eclogites (Schuster et al., 2004; Teiml, 1996), but there are differences, in lithological as well as structural aspects. Additionally, Hoinkes et al. (1999) pointed out the similarities between the LU west and the MC east of the TW.

From Teiml (1996), thermobarometric data indicate eclogite facies conditions (580 – 600°C and 12 - 13kbar minimum pressures) for the MC. The TC shows P/T-conditions of 540 - 620°C and 12 – 14kbar (Habler, 2006) reaching 640 - 680°C at similar pressures after Poli (1991). Contrasting, samples from the Ulfas-valley, taken from retrogressed eclogites from the southernmost TC, show even higher UHP metamorphic conditions up to 630 – 690°C and 26 – 29 kbar (Zanchetta et al., 2007; Fig. 31)

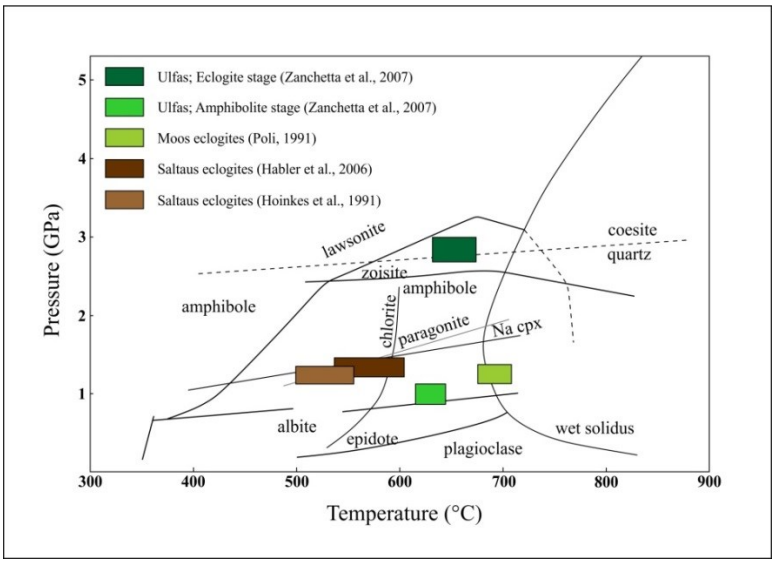

Fig. 31|P/T diagram showing thermobarometric data from the TC, from various localities and authors. (after Zanchetta et al., 2007)

This study proposes the MC to be the equivalent unit of the LU west of the TW. The facts supporting this view are: (I) both show a polymetamorphic evolution; (II) both units bear massive tremolite-marbles with relictic diopside and (III) both units contain pegmatites of Permian age which clearly lack in the TC below (Hoinkes et al., 1999).

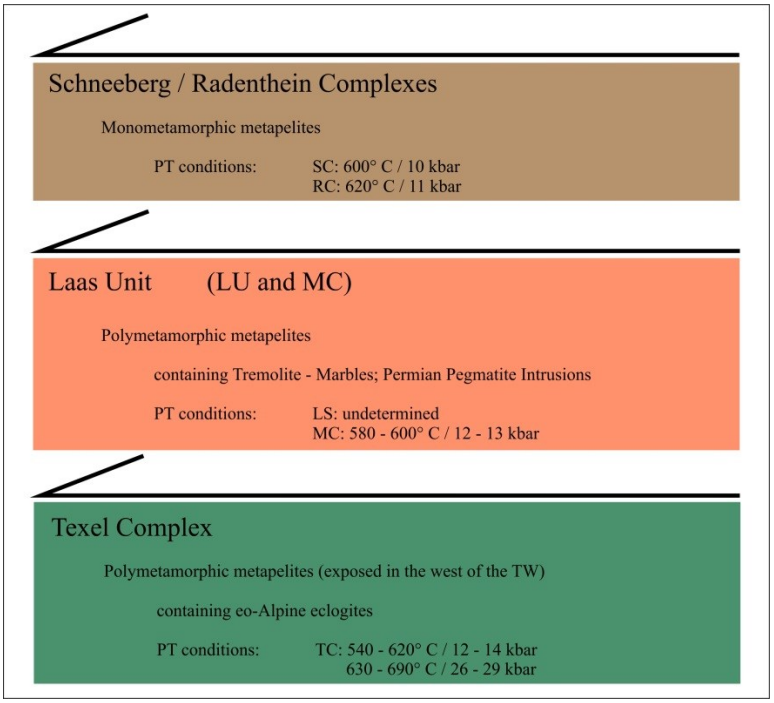

Fig. 31| Schematic tectonostratigraphic succession of KWNS, east and west of the TW.

In addition to these arguments, the similarities between the MC and LU, both show the "Laas Type" garnet zonation, supports this view. Heinisch (2014) observed this pattern south of the SC (Garnet types 3a, 3b and 4), which coincide with garnets from the MC (samples MI30, MI48 and MI32). Cores show higher X_{Grs} values, whereas rims show a decrease in the Ca contents. From studies in the ÖBN and Wölz and Rappold units (e.g. Schuster and Thöni, 1996; Schuster and Frank, 1999; Koroknai et al., 1999; Faryad and Hoinkes, 2003) the eo-Alpine signature in garnets is typically represented by a "jump" due to an increase in the X_{Grs} component towards the rims. This contradiction is argued to be linked to the amount of free Ca in the bulk chemistry. The chemical profile from sample MI30 (Fig. 30) shows the correlation between X_{Grs} contents in garnet during staurolite breakdown. A possible process can be proposed, that simultaneous prograde breakdown of permian staurolite during eo-Alpine metamorphism greatly affects the amount of Ca incorporated into the garnets. This means that the Ca abundance is very limited within the MC and LU. This process, however, was discussed earlier in the units west of the TW (Heinisch, 2014).

Massive marbles are described in the LU, consisting of comparable mineral assemblages, east and west of the TW (Konzett, 1990; Puhr, 2009). Furthermore, such marbles are found throughout various units of the KWNS, e.g. Rappold and Wölz units, Koralpe-Saualpe and Pohorje Complexes (Schmid et al. 2004).

The TC contains no pegmatitic melts, no massive marble layers and also higher P/T conditions for the eclogite assemblages, and is therefore not interpreted as positioned in the same nappe unit to the MC within the KWNS. A further assumption could be that eclogites from the TC do not stem from Permian protoliths representing a separate nappe unit from all eclogites of the KWNS further east of the TW, where they occur associated with Permian pegmatites and massive marbles.

From pre-existing mappings of the RC (performed by the Austrian Geological Survey, GBA), a schematic tectonic profile from the southern BC toward the southeast has been reconstructed, indicating the syn- and antiform internal architecture within the KWNS. The MF limits the southern extent of the KWNS. To the north it is overlain by the BC, which was located on upper-plate position during the eo-Alpine event (Krenn et al., 2011).

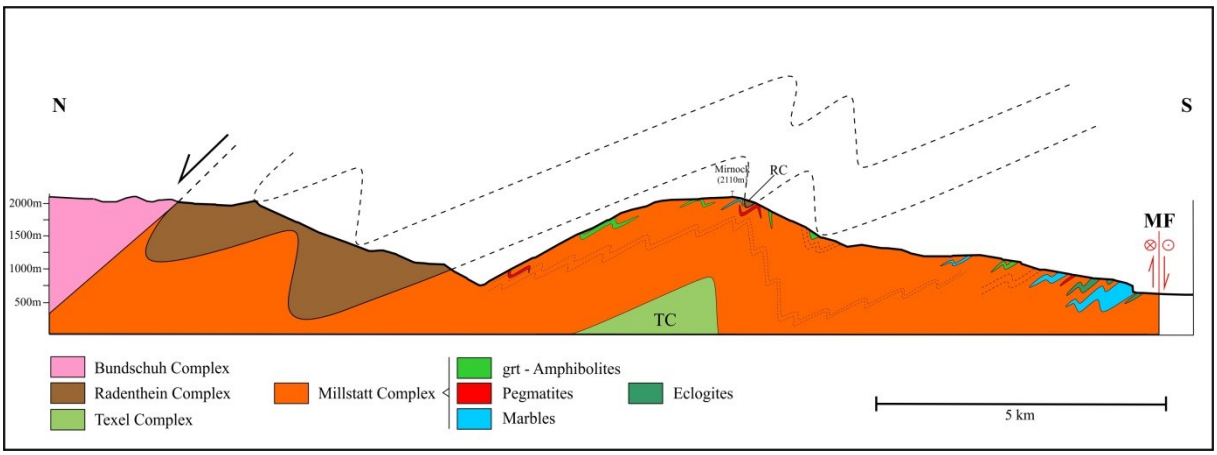

Fig. 33| Schematic cross-section of the BC, RC, MC and TC, east of the TW.

The major large-scale folding is simplified in figure 33. The BC in the hangingwall position to the RC is separated by a normal fault. After Schuster and Frank (1999), a small portion of the RC lies on top of the MC, south from the Mirnock summit. This has been implemented into the tectonic sketch.

Considering the evolution of the Eastern Alps, the KWNS underwent tectonometamorphism characterized by subduction, exhumation together with large-scale folding during the eo-Alpine and subsequent re-orientation during the Alpine indentation and unroofing process of the TW. Figures 34 a and b illustrate the position of the TC, MC and RC during these two processes.

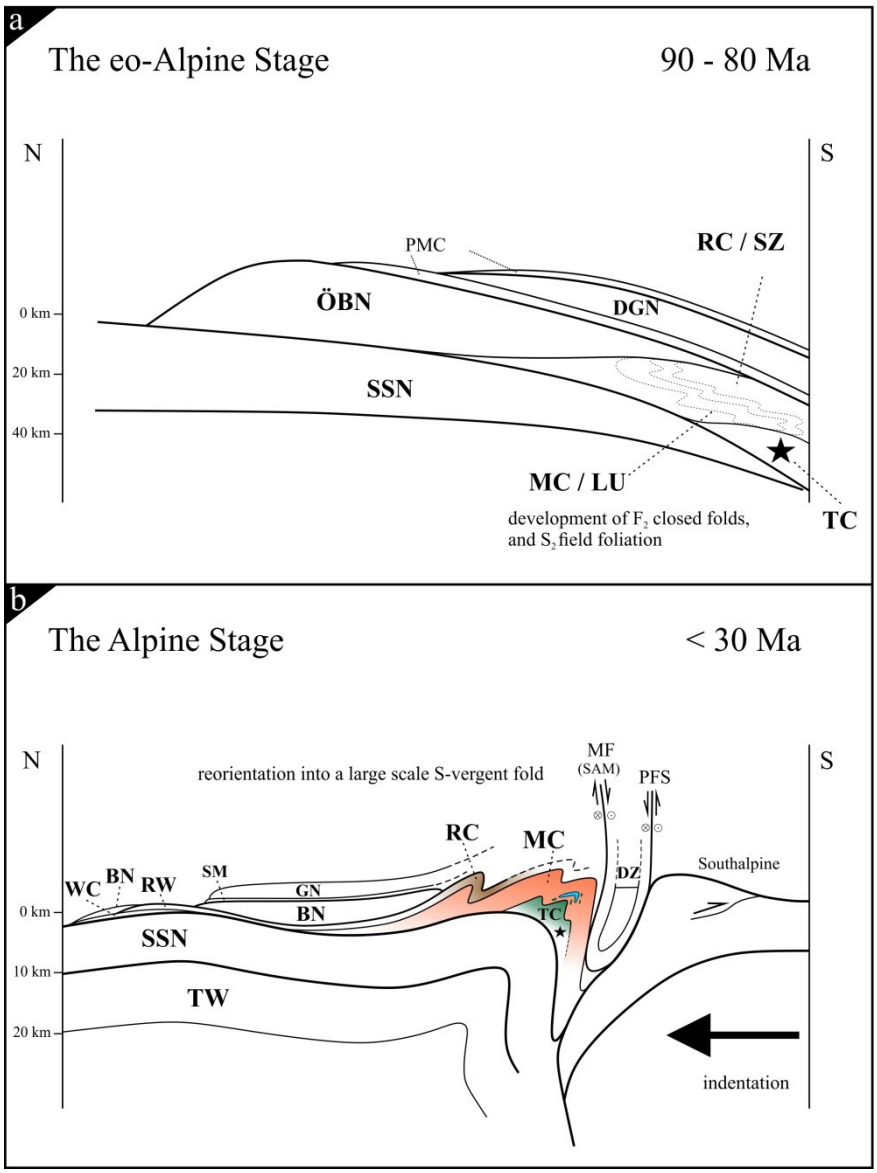

Fig. 34| **a)** Tectonic position of the eo-Alpine wedge, showing units and folding stage F1, for units East and West of the TW; **b)** Tectonic profile across the Alpine orogen, east of the TW, displaying units and fold geometry F2 developed during indentation of the Southalpine in Eocene Times. Simply modified after Krenn et al. 2011. ÖBN: Ötztal Bundschuh Nappe; DGN: Drauzug-Gurktal Nappe; PMC: Permomesozoic Cover; SSN: Silvretta-Seckau Nappe; RC: Radenthein Complex; SZ: Schneeberg Complex; MC: Millstatt Complex; LU: Laas Unit; TC: Texel Complex; WC: Wölz Complex; BN: Bundschuh Nappe; RW: Ramingstein Window; SM: Stangalm Mesozoic; GN: Gurktal Nappe; DZ: Drau-Zug; TW: Tauern Window.

Conclusions

The Millstatt Complex, attributed to the KWNS, represents a polymetamorphic, metasedimentary unit including Permian pegmatoid melts reflecting wedge tectonics and re-orientation during the eo-Alpine and Alpine metamorphic events, respectively. Early Cretaceous structures involve the development of S_1 and L_1 structures, as well as tight F_1 folds, which were incorporated into a large-scale F_2 fold structure and an associated penetrative S_2 field foliation. The whole unit was re-oriented due to indentation tectonics, resulting into almost SSW-vergent re-orientated F_2 fold structures. Re-orientation led to variable dip angles for field foliations and fold surface planes in the field.

This study supports arguments that the unit may be comparable to the Laas Unit in the west of the Tauern Window. Both units bear massive tremolite marbles, and were injected by pegmatoid melts during the Permian event. Selective garnets from metapelitic units of the MC and LU show a characteristic garnet zonation type, which is here defined as the "Laas type" (see also Heinisch, 2014). This contrasts to the currently proposed garnet zonation patterns of Permian and eo-Alpine garnet zonation types which are characterized as almandine-rich garnets with higher X_{Grs} values in the core, which rise abruptly at the rims (Heinisch, 2014; Schuster and Frank, 1999; Faryad and Hoinkes, 2002). The "Laas type" zonation may be related to bulk chemical arguments of staurolite of Permian age or simply the effect of the marble units nearby which control the amount of Ca within the surrounding metapelites. However, age data to support this new tectonic nappe distinction are missing and have to be prepared in the future to support this argument.

References

Faryad, S.W. and Hoinkes, G. (2003), P-T gradient of Eo-Alpine metamorphism within the Austroalpine basement units east of the Tauern Window (Austria). *Mineralogy and Petrology* (77) 129 – 159; DOI 10.1007/s00710-002-0196-1.

Frisch, W., Dunkl, I., & Kuhlemann, J. (2000). Post-collisional orogeny-parallel large scale extension in the Eastern Alps. *Tectonophysics*, 327, pp. 239-2265

Froitzheim, N., Schmid, S. M., & Conti, P. (1994). Repeated change from crustal shortening to orogen-parallel extension in the Austroalpine units of Graubünden. *Eclogae geologicae Helveticae*, 87, pp. 559-612

Habler, G., Thöni, M., & Sölva, H. (2006). Tracing the high pressure stage in the polymethamorphic Texel Complex (Austroalpine basement unit, Eastern Alps): P-T-t-d constraints. *Mineralogy and Petrology (88)*, pp. 269-296.

Habler, G., & Thöni, W. (2001). Preservation of Permo±Triassic low-pressure assemblages in the Cretaceous high-pressure metamorphic Saualpe crystalline basement (Eastern Alps, Austria). *Journal of Metamorphic Petrology (19)*, pp. 679-697.

Handy, M. R., Schmid, S., Bousquet, R., Kissling, E., Bernoulli, D. (2010). Reconciling plate-tectonic reconstructions of Alpine Tethys with the geological–geophysical record of spreading and subduction in the Alps. *Earth-Science Reviews (102) pp. 121–158.*

Heinisch, M. (2014). Petrologische Untersuchungen im Übergangsbereich zwischen Ötztal-Bundschuh Deckensystem und Koralpe-Wölz Hochdruckdeckensystem westlich des Tauernfensters (Tirol, Österreich); *Unpublished Master Thesis*. Karl-Franzens University Graz.

Hoinkes, G., Koller, F., Rantitsch, G., Dachs, E., Höck, V., Neubauer, F., et al. (1999). Alpine Metamorphism of the Eastern Alps. *Schweizerische Mineralogische und Petrographische Mitteilungen*(79), pp. 155-181.

Hoinkes, G., Kostner, A., & Thöni, M. (1991). Petrologic constraints for Eoalpine eclogite facies metamorphism in the Austroalpine Ötztal basement. *Mineralogy and Petrology*(43), pp. 237- 254.

Janàk, M., Froitzheim, N, Lupták, B., Vrabec, M., & Krogh Ravna, E. J. (2004). First evidence for ultrahigh-pressure metamorphism of Eclogites in Pohorje, Slovenia: Tracing deep continental subduction in the eastern Alps. *Tectonics*, 23, TC5014. doi: 10.1029/2004TC001641.

Konzett, J. (1990). Petrologie des zentralen Schneeberger Zugs und des südlich angrenzenden Kristallins im Bereich der Hohen Kreuzspitze, Passeiertal, Südtirol. *Unpublished PhD Thesis, Leopold-Franzens-Universität Innsbruck*.

Koroknai, B., Neubauer, F., Genser, J., & Topa, D. (1999). Metamorphic and tectonic evolution of Austroalpine units at the western margin of the Gurktal nappe complex, Eastern Alps. *Schweiz. Mineral. Petrogr. Mitt.* (79), pp. 277-295

Krenn, K., Kurz, W., Fritz, H., & Hoinkes, G. (2011). Eoalpine tectonics of the Eastern Alps: implications from the evolution of monometamorphic Austroalpine units (Schneebergzug and Radenthein Complex). *Swiss Journal of Geosciences (104)*, pp. 471-491.

Kurz, W., Handler, R., Bertoldi, C. (2008). Tracing the exhumation of the Eclogite Zone (Tauern Window, Eastern Alps) by $^{40}Ar/^{39}Ar$ dating of white mica in eclogites. *Orogenic Processes in the Alpine Collision Zone; Volume 3 of the series Swiss Journal of Geosciences Supplement,* pp. S191-S206; doi. 10.1007/978-3-7643-9950-4_11

Kurz, W., Unzog, W., Neubauer, F. (2001). Evolution of quartz microstructures and textures during polyphase deformation within the Tauern Window (Eastern Alps). *Int J Earth Sci* , 90: 361. doi:10.1007/s005310000153

Micheuz, P. (2014). Structural and petrological studies of two selected high-pressure units within the Alpine orogen (External Hellenides, Eastern Alps). *Unpublished Master Thesis, Technical University Graz*.

Pomella, H., Flöss, D., Speckbacher, R., Tropper, P., & Fügenschuh, B. (2015). The western end of the Eoalpine High-Pressure Belt (Texel unit, South Tyrol / Italy).*Terra Nova*, 28, pp. 60-69

Puhr, B., Hoinkes, G., Proyer, A., & Schuster, R. (2009). Petrology of metacarbonate rocks of the Austroalpine basement east of the Tauern Window (Austria). *Mitteilungen der Österreichischen Mineralogischen Gesellschaft*, 155, p.134.

Schimana, R. (1986). Neue Ergebnisse zur Entwicklungsgeschichte des Kristallins um Radenthein (Kärnten, Österreich). Mitt. Ges. Geol. Bergbaustud. Österr.; 33; pp. 221-232

Schmid, S., Fügenschuh, B., Kissling, E., & Schuster, R. (2004). Tectonic map and overall architecture of the Alpine orogen. *Eclogae geologicae Helvetiae* (97), pp. 93-117.

Schuster R., Frank, W. (1999). Metamorphic evolution of the austroalpine units east of the Tauern Window: indications for Jurassic strike slip tectonics. *Mitt. Ges. Geol. Bergbaustud. Österr*. 42, pp. 37-58.

Schuster, R., Koller, F., Hoeck, V., Hoinkes, G., & Bousquet, R. (2004). Metamorphic evolution of the Eastern Alps. *Mitteilungen der Österreichischen Mineralogischen Gesellschaft (149)*, pp. 175-199.

Schuster, R., & Thöni, M. (1996). Permian garnets: indication for a regional Permian metamorphism in the southern part of the Austroalpine basement units. *Mitteilungen der Österreichischen Geologischen Gesellschaft*, *141*, 219-221.

Spear, F. S. (1993). Metamorphic Phase Equilibria and Pressure-Temperature-Time Paths. *Mineralogical Society of America*.

Strauss H. (1990). Kristallisations- und Deformationsgeschichte des Altkristallins nordwestlich von Villach. (*PhD Thesis*) Karl-Franzens-University, Graz.

Teiml, X. & Hoinkes, G. (1996). Der P-T Pfad der Millstätter Serie und ein Vergleich mit dem südlichen Ötztal – Stubai - Kristallin. *Mitteilungen der Österreichischen Mineralogischen Gesellschaft*, 141, pp. 228-229.

Zanchetta, S., Salvi, F., Zanchi, A., & Poli, S. (2007). Structural aspects of the Texel-Schneeberg boundary in the Pfossen valley (Central Eastern Alps, NE Italy). *Mitteilungen der Österreichischen Mineralogischen Gesellschaft,* 153.

Appendix

1. Table with sample locations, rock type and S and L values

S	Lat	Lon	Gestein	Schieferung		Lineation	
				Strike	Dip	Strike	Dip
MI01	46,6509579	13,81030446	Grt-Amphibolit	150	65	173	36
	46,6509579	13,81030446	Grt-Amphibolit	130	50		
	46,6509579	13,81030446	Grt-Amphibolit	155	45		
MI02	46,6509579	13,81030446	Grt-Amphibolit				
MI03	46,65213196	13,80891097	Grt Glimmerschiefer				
MI04	46,65213196	13,80891097	Grt-Amphibolit				
MI05	46,65580717	13,80533332	Grt Glimmerschiefer	20	22	90	10
MI06	46,65634914	13,80832817	Grt Glimmerschiefer	354	30	284	10
MI07	46,65634914	13,80832817	Grt Glimmerschiefer				
MI08	46,65827958	13,81482306	Pgm	40	15		
MI09	46,65561673	13,8115102	Grt Glimmerschiefer				
MI10	46,65561673	13,8115102	Grt Glimmerschiefer	55	12	132	20
	46,65561673	13,8115102	Grt Glimmerschiefer	63	40		
MI11	46,65690721	13,80101832	Amphibolit	45	45	95	30
MI12	46,65690721	13,80101832	Grt-Amphibolit	70	20	95	25
MI13	46,65690721	13,80101832	Grt Glimmerschiefer				
MI14	46,65004252	13,81065583	Marmor	340	80		
MI15	46,67757028	13,81680169	Met. Kalksilikat				
MI16	46,67757028	13,81680169	Grt/Hbl Glimmerschiefer				
MI17	46,67757028	13,81680169	Grt/Hbl Glimmerschiefer				
MI18	46,67757028	13,81680169	Grt 2G Schiefer				
MI19	46,74589662	13,72301674	Grt Glimmerschiefer				
	46,74589662	13,72301674					
MI20	46,74546428	13,7239634	Grt 2G Schiefer	355	82	80	45
MI21	46,74997198	13,7255713	Glimmerschiefer	145	40	170	30
MI22	46,74997198	13,7255713	Grt – Amphibolit	145	77	56	35
MI23	46,74997198	13,7255713	Amphibolit				
MI24	46,72120018	13,66464584	Pgm				
MI25	46,72120018	13,66464584	Grt 2G Schiefer				
MI26	46,76601553	13,64628998	Pgm	25	32		
MI27	46,79289211	13,70824381	Grt 2G Schiefer				
	46,79289211	13,70824381					
	46,79289211	13,70824381					
MI28	46,79194411	13,70462392	Grt 2G Schiefer	190	24	125	20
	46,79194411	13,70462392		190	28		
MI29	46,7861414	13,70635386	Grt 2G Schiefer				
MI30	46,76836062	13,70304518	Grt 2G Schiefer	108	40	90	35
	46,76836062	13,70304518		110	40		
MI31	46,75980454	13,71480122	Grt – Amphibolit	174	45	114	26
MI32	46,76239111	13,58716789	St-Grt Glimmerschiefer	350	15	312	20

	46,76239111	13,58716789		29	13		
	46,76239111	13,58716789		4	22		
	46,76239111	13,58716789		349	15		
MI33	46,76764749	13,58377623	Grt 2G Schiefer	345	9	323	12
	46,76764749	13,58377623		343	30	343	10
	46,76764749	13,58377623		10	19		
	46,76764749	13,58377623		6	20	324	11
MI34	46,74836425	13,68427609	Grt – Amphibolit	322	17	78	15
	46,74836425	13,68427609		305	20	90	20
MI35	46,76933753	13,70311065	Glimmerschiefer	194	85		
MI36	46,76799324	13,69969913	Grt-Glimmerschiefer/Pgm	320	60		
	46,76799324	13,69969913		322	58		
	46,76799324	13,69969913		300	70		
MI37	46,76799324	13,69969913	Grt-Glimmerschiefer/Pgm	324	60	250	15
MI38	46,76799324	13,69969913	Pgm				
MI39	46,76580423	13,70324115	2G Schiefer	320	80	345	25
MI40	46,761883	13,70847029	Grt 2G Schiefer	20	87	286	30
	46,761883	13,70847029	Glimmerschiefer	22	80	294	20
MI41	46,75908471	13,7150645	Grt-Glimmerschiefer	178	60	106	5
MI42	46,75908471	13,7150645	Grt-Glimmerschiefer	173	50	84	25
MI43	46,75908471	13,7150645	2G Schiefer	170	50	92	20
MI44	46,76917794	13,71368056	Grt 2G Schiefer	114	15	140	10
	46,76917794	13,71368056		108	15	138	10
	46,76917794	13,71368056		128	25		
MI45	46,76904467	13,71384795	Grt 2G Schiefer	150	15	116	20
MI46	46,76904467	13,71384795	Quarzit	146	20	110	15
MI47	46,75599019	13,71273885	Marmor	160	42	98	25
MI48	46,75495117	13,7127267	Grt-Glimmerschiefer	164	50		
MI49	46,75472746	13,71284564	Amphibolit	158	37	90	15
MI50	46,75449771	13,71385105	2G Schiefer	154	45	78	12
MI51	46,7523584	13,71014181	Grt 2G Schiefer	348	89	78	10
				354	70		
MI52	46,7523584	13,71014181	Glimmerschiefer / Amphibolit	354	90	84	10
MI53			Grt-Amphibolit				
MI54			Grt-Amphibolit				
MI55	46,78222815	13,69763919	Grt-Amphibolit				
MI56	46,78011859	13,71171777	Grt-Amphibolit				
MI57	46,80197088	13,6883305	Grt 2G Schiefer	18	75	292	10
	46,80197088	13,6883305					
	46,80197088	13,6883305					
	46,80197088	13,6883305					
MI58	46,80163954	13,68600125	Glimmerschiefer	334	35	262	15
MI58a	46.68677777	13.72502777	Q, Bt – Glimmerschiefer	12	45	40	35
MI59	46.68677777	13.72502777	Marmor / Amphibolit	6	50		
MI60	46.68677777	13.72502777	Grt-Bt-Glimmerschiefer	40	25	24	20

MI61	46.68677777	13.72502777	Amphibolit	10	85		
MI62	46.68677777	13.72502777	2G Schiefer	24	25	52	20
MI63	46.68677777	13.72502777	Q – Ader	24	60	63	30
MI64			Grt-Amphibolit (findling)				
MI65	46,714263	13,779453	Grt-Quarzit	20	30	310	5
	46,714263	13,779453		24	36		
MI66	46,713173	13,777387	Grt-Glimmerschiefer	4	30	332	20
	46,713173	13,777387					
MI67	46,710961	13,7783	Grt-Glimmerschiefer RC?				
MI68	46,710075	13,775599	Grt-Glimmerschiefer	208	60	296	10
	46,710075	13,775599		200	80		
MI69	46,707298	13,758258	Grt-Glimmerschiefer	204	40	272	15
	46,707298	13,758258		204	25	268	15
MI70	46,7412	13,781614	Grt-Glimmerschiefer RC?	50	30	124	5
	46,7412	13,781614		50	35	116	15
MI71	46,691545	13,795292	Pgm	112	40	124	35
MI72	46,691685	13,796178	Q Grt-Glimmerschiefer	172	30	112	15
MI73	46,691685	13,796178	Q Grt-Glimmerschiefer	140	25	116	20
MI74	46,690762	13,798302	Grt-Glimmerschiefer	90	30	36	10
MI75	46,690762	13,798302	Grt-Bt Glimmerschiefer	116	30	146	20
MI76	46,690762	13,798302		174	55	244	35
MI77	46,710597	13,809581	Quarzit	130	30	92	30
	46,710597	13,809581		100	33	90	25
MI78	46,710981	13,810676		76	15	80	15
	46,710981	13,810676		90	20	84	25
MI79	46,752319	13,672674	Glimmerschiefer	44	30	90	20
	46,752319	13,672674		35	25	102	30
	46,752319	13,672674		25	36		
MI80	46,759532	13,689157	Bt – Glimmerschiefer	16	65	304	20
MI81	46,759532	13,689157	Amphibolit	16	55	272	22
MI82	46,759532	13,689157	Amphibolit	9	55		
MI83	46,760688	13,688017	Bt – Glimmerschiefer	20	55	356	35
	46,760688	13,688017	Bt – Glimmerschiefer	18	55	344	35
	46,760688	13,688017	Bt – Glimmerschiefer	14	45	30	50
MI84	46,757546	13,690785	Amphibolit	12	65	96	25
MI85	46,75329	13,702726	Grt-Glimmerschiefer	48	33	96	25
MI86	46,75229	13,679347	Grt-Bt Glimmerschiefer	28	35	114	20
				14	20	112	10
MI87	46,7622264	13,587035	Grt-Glimmerschiefer	8	50	94	15
	46,7622264	13,587035				288	10
MI88	46,780001	13,584362	Grt Bt-Glimmerschiefer	338	35	52	12
MI89	46,775253	13,577613	Glimmersciefer	358	33	272	13
MI94	46,767569	13,584033	Q Grt-Glimmerschiefer	342	15	310	10
	46,767569	13,584033	Q Grt-Glimmerschiefer	344	20	62	20
	46,767569	13,584033	Q Grt-Glimmerschiefer	20	22	332	12

MI90	46,708009	13,755997	Grt-Glimmerschiefer	194	25	270	10
	46,708009	13,755997		186	26	272	10
MI91	46,704989	13,740363	Glimmerschiefer	30	33	308	8
	46,704989	13,740363		30	45	90	23
MI92	46,705518	13,739181	Glimmerschiefer	102	10	126	5
	46,705518	13,739181		58	17		
	46,705518	13,739181		54	20		
MI93	46,705518	13,739181	Glimmerschiefer	56	26	72	20
MI95	46.73890830	13.71911760	Grt – Amphibolit	158	25	92	5
MI96	46.70111090	13.72435380	2G Schiefer	12	45	310	15
MI97	46.70304800	13.72138840	Glimmerschiefer	360	45	60	30
MI98	46.70674310	13.71628920	Amphibolit	356	35	66	10

2. Structural Map